INL/EXT-20-40088
Revision: 1

Baseline Postirradiation Examination of the FUTURIX-FTA Experiments

Fuel Cycle Research & Development
Advanced Fuels Campaign

Jason M. Harp
Heather J.M. Chichester
Luca Capriotti

Prepared for
U. S. Department of Energy
Office of Nuclear Energy

September 2016
FCRD-Fuel-2016-000034

Rev.1 May 2020

INL/EXT 20-40088
Revision 1

Baseline Postirradiation Examination of the FUTURIX-FTA Experiments

Jason M. Harp
Heather J.M. Chichester
Luca Capriotti

September 2016

Rev. 1 May 2020

Idaho National Laboratory
Idaho Falls, Idaho 83415

http://www.inl.gov

Prepared for the
U.S. Department of Energy
Office of Nuclear Energy
Under DOE Idaho Operations Office

Contract DE-AC07-05ID14517

INTENTIONALLY BLANK

CONTENTS

FIGURES

TABLES

Baseline Postirradiation Examination of the FUTURIX-FTA Experiment

1. Introduction

Postirradiation Examination (PIE) results from the baseline examination of the FUTURIX-FTA irradiation experiment are presented in this report. The FUTURIX-FTA irradiation was designed to study the fuel performance of candidate transmutation fuels. The FUTURIX-FTA experiment was conducted in the true fast neutron spectrum conditions of the Phénix sodium fast test reactor in France. FUTURIX-FTA contained several compositions that were also irradiated as part of the AFC-1 test in cadmium filtered positions in the Idaho National Laboratory (INL) Advanced Test Reactor (ATR) that approximate the neutron spectrum of a fast reactor [1, 2]. This experiment was a joint collaboration between the Department of Energy (DOE) in the U.S. and the Commissariat à l'Energie Atomique et aux Energies Alternatives (CEA) in France. A joint agreement between DOE and CEA was established in 2004 to conduct an irradiation experiment of metallic and nitride fuels in the Phénix reactor at CEA. Both the FUTURIX-FTA tests and the AFC-1 tests were conducted for the DOE Advanced Fuels Campaign (AFC) that is part of Fuel Cycle Research & Development (FCRD) program. These programs seek to develop and demonstrate the technologies needed to transmute long-lived transuranic actinide isotopes contained in spent nuclear fuel via fast reactor technology. The long term goal of this work is to reduce the radiotoxicity of future high level waste repositories. Postirradiation examination of irradiated fuels experiments provides data related to in reactor fuel performance and input into future fuel design choices [3]. The compositions of the FUTURIX-FTA pins were designed to test if minor actinides could be incorporated into the fuel of a fast reactor without significantly changing fuel performance observed for previously well studied fuels. The fuel performance of metallic fuel in fast reactors has been well documented [4, 5, 6, 7, 8]. Likewise the irradiation performance of nitride fuels in fast reactors has also been documented. However the existing database for nitride fuels is much smaller than the database for metal fuels [9].

The FUTURIX-FTA irradiations provide a validation case that helps validate if ATR pseudo-fast spectrum testing adequately reproduces fuel performance behavior in a true fast spectrum reactor like Phénix or if there are tangible differences that need to be considered when evaluating fuel performance based on ATR testing. Pins consisted of a 35.2 cm miniature fuel rod (rodlet) with extensions welded to the top and bottom of each rodlet. A sketch of the fuel rodlet is shown in Figure 1. Compositions and sister AFC-1 rodlets are listed in the Table 1. Metallic fuel pins achieved burnups of 9.1 at.% HM (DOE1) and 15.5 at% HM (DOE2). Nitride fuel pins achieved burnups of 1.6 at.% HM (DOE 3) and 4.1 at.% HM (DOE 4). Postirradiation Examination (PIE) of FUTURIX-FTA occurred at the INL Hot Fuel Examination Facility (HFEF) hot-cell. [10]

Baseline PIE is now complete for the FUTURIX-FTA Pins. All indications are the fuel performed well during the irradiation. These exams include visual inspection of the pins, neutron radiography, dimensional inspection of the fuel pin diameter, gamma spectrometry examination of the pins, fission gas release analysis, optical microscopy and chemical burnup analysis. The results of all these exams will be summarized in this report.

Table 1. Composition of FUTURIX Rodlets and Sister AFC-1 Rodlets

Name	Fuel Type	Composition*	AFC Rodlets
DOE1	Metallic low fertile	U-28.3Pu-3.8Am-2.1Np-31.7Zr	AFC-1F: 1, 4 AFC-1H: 1, 4
DOE2	Metallic non-fertile	Pu-10.5Am-0.3Np-41.6Zr	AFC-1B: 1, 4 AFC-1D: 1, 4 AFC-1G: 1, 4
DOE3	Nitride low fertile	$(U_{0.51}Pu_{0.27}Am_{0.14}Np_{0.08})N$	AFC-1Æ: 1, 3, 4
DOE4	Nitride non-fertile	$(Pu_{0.85}Am_{0.15})N+46.5ZrN$	AFC-1Æ: 6 AFC-1G: 3

*numbers preceding elements denote weight percent, subscript numbers represent mole percent. This is the as-fabricated composition not the nominal composition

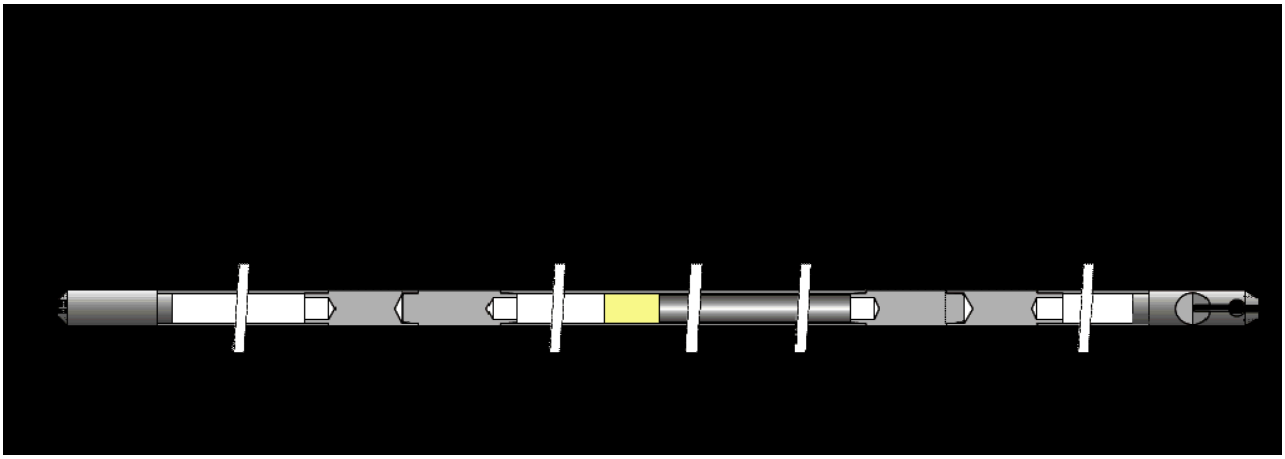

Figure 1. FUTURIX-FTA rodlet configuration and dimensions

2. Fabrication and Irradiation History

Fuels for the FUTURIX-FTA experiment were fabricated in the U.S. The metallic fuels were fabricated at INL and the nitride fuels were fabricated at Los Alamos National Laboratory (LANL). Short experimental fuel pins were assembled and welded at INL and shipped to CEA in 2006 where extensions were welded onto the short pins to make them the same length as standard Phénix fuel pins. A schematic of the fuel pins with extensions is shown in Figure 1.

The short fuel pins were 352 mm in length with ~100 mm fuel column. In the metallic fuel pins, sodium was included in the fuel-cladding gap for metallic and nitride pins to improve heat transport between the fuel and the cladding and improve the fuel thermal behavior. The fuel pin cladding is AIM1 [11, 12], an austenitic stainless steel provided by CEA as the standard Phénix cladding. Fuel pin parameters are listed in Table 2.

Table 2. FUTURIX-FTA Pin Parameters

Parameter	Value
Cladding	AIM1
Fuel Pin Inner Diameter	5.65 mm (0.222 in.)
Fuel Pin Outer Diameter	6.55 mm (0.258 in.)
Fuel Column Length	100 mm (3.93 in.)
Short Fuel Pin Length	352 mm (13.8 in.)
Full Fuel Pin Length	1793 mm (70.6 in.)

The FUTURIX-FTA experimental fuel pins were assembled into two Phénix fuel capsules and placed into adapted assemblies. Each Phénix fuel capsule contained 19 fuel pins. Capsule KCI 6908 housed two metallic fuel experimental pins, DOE-1 and DOE-2, and capsule KCI 6909 had two nitride fuel experimental pins, DOE-3 and DOE-4. The remaining 17 fuel pins in each capsule were Phénix standard fuel pins.

2.1 Metallic Fuels

Two metallic fuel compositions were fabricated at INL in 2006. The metallic fuel slugs were fabricated using an arc-casting method where the individual feedstock materials are melted together and homogenized into a "button." The button was melted, an uncoated quartz tube mold was dipped into the liquid, and the liquid was drawn up into the model via suction using a syringe [13]. The final metallic fuel slugs are shown in Figure 2 and Figure 3

Samples from representative casts of the fuel alloy compositions were characterized for phase formation by X-ray diffraction (XRD), microstructure by scanning electron microscopy (SEM), heat capacities and thermal phase transitions by Differential Scanning Calorimetry (DSC) and Differential Thermal Analysis (DTA) measurements, thermal expansion from Thermomechanical Analysis (TMA) measurements, thermal diffusivity by the laser flash method, thermal conductivity. Fuel alloy resistance to fuel-cladding-chemical-interaction (FCCI) with the AIM1 stainless steel cladding material was tested with a series of diffusion couples [13].

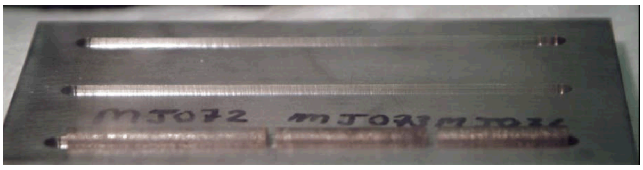

Figure 2. Fuel column of the U-29Pu-4Am-2Np-30Zr composition prior to DOE-1 fuel pin loading.

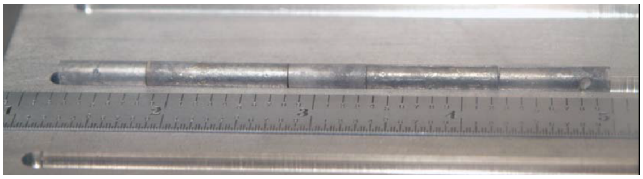

Figure 3. Fuel column of the Pu-12Am-40Zr composition prior to DOE-2 fuel pin loading.

2.2 Nitride Fuels

Two nitride fuel compositions were fabricated at LANL in 2006. The nitride fuel pellets were fabricated using carbothermic reduction/nitridization (CTR/N) to convert feedstock material and solutions from an oxide to a nitride. The nitride solution feedstock was then milled, pressed into pellets and sintered [14]. Selections of the nitride fuel pellets and property measurement samples are shown in Figure 4 and Figure 5.

Figure 4. Low-fertile nitride pellets and property measurement samples for the DOE-3 fuel pin.

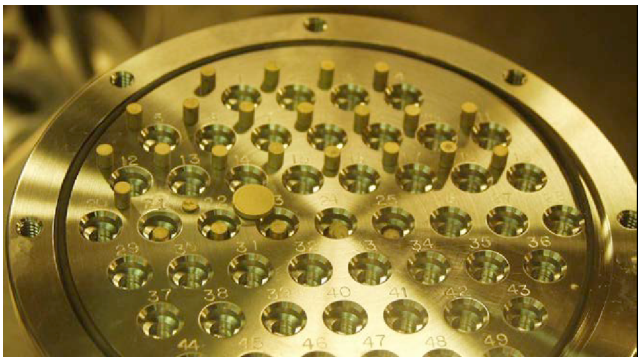

Figure 5. Non-fertile nitride pellets and property measurement samples for the DOE-4 fuel pin.

In addition to the fuel pellets, several fuel samples were fabricated for material property measurements. Characterization of fuel pellets and/or property samples included visual inspection, dimensional inspection, density, thermal diffusivity, thermal expansion, calorimetry, optical microscopy, phase formation by X-ray diffraction, and microstructure by scanning electron microscopy [14].

Fabrication development for nitride fuel pellets containing minor actinides encountered significant challenges. The americium oxide feedstock for the FUTURIX-FTA fuels appeared to be different than the feedstock previously used for the AFC-1 fuel fabrication, so additional heat treatments were applied to the feedstock to remove moisture

and improve flowability. Smaller batch sizes were used during the fabrication process to reduce handling and storage time for the feedstock.

Limited fabrication development time prevented fuel pellet fabrication process optimization. Delamination and end-capping were observed in the non-fertile fuel pellets. Process improvements were identified and tested and the final pellets were fabricated using the recommended process parameters. Details of the fertile and non-fertile nitride fuel fabrication are described in a fuel fabrication report [14].

All pellets selected for the irradiation experiment met fuel fabrication specification criteria for density and physical defects; however, given that the fuel densities were on the lower end of the specification range, pellets were prone to cracking during fabrication, and the fact that irradiation performance data for actinide-bearing nitride fuels was limited, the irradiation duration was constrained to prevent fuel swelling and hard contact with the cladding.

2.3 Irradiation

The metallic fuel pins met all of their fabrication and inspection acceptance criteria and were accepted for their planned irradiation. The metallic fuel pins, DOE-1 and DOE-2, began irradiation in May 2007 and completed irradiation in May 2009 for a total of 235 EFPD. No sign of fuel pin failure (i.e., loss of tightness) was detected during irradiation [15].

Fabrication of the minor actinide-containing nitride fuels produced pellets that were less robust than desired and prone to cracking. Based on concerns about the integrity of the fuel, the irradiation duration was limited to prevent fuel swelling [16].

The nitride fuel pins, DOE-3 and DOE-4, began irradiation in July 2008 and completed irradiation in November 2008 for a total of 56 EFPD. No sign of fuel pin failure (i.e., loss of tightness) was detected during irradiation. A summary of burnup for the four FUTURIX-FTA pins is shown in Table 3.

Table 3. FUTURIX-FTA Fuel Pin Predicted Burnup

Pin	Fuel Composition*	Burnup (at% HM)	Fission Density (fissions/cm^3)
DOE-1	U-28.3Pu-3.8Am-2.1Np-31.7Zr	9.1	1.99×10^{21}
DOE-2	Pu-10.5Am-0.3Np-41.6Zr	15.5	2.46×10^{21}
DOE-3	$(U_{0.51}Pu_{0.27}Am_{0.14}Np_{0.08})N$	1.6	4.95×10^{20}
DOE-4	$(Pu_{0.85}Am_{0.15})N+46.5ZrN$	4.1	4.78×10^{20}

* DOE-1 and DOE-2 composition expressed in weight %.
DOE-3 and DOE-4 composition expressed in mole fraction.

Following the completion of irradiation and the shutdown of the Phénix reactor, the FUTURIX-FTA experiments were stored in a transfer drum. In March 2014 the assemblies containing the FUTURIX-FTA pins were transferred into the Phénix hot cell, washed, and disassembled. The four FUTURIX-FTA pins were visually verified and inserted into an ET-004 basket prior to loading in a TN-106 cask for shipment to the U.S. In July 2014, the TN-106 cask with the FUTURIX-FTA pins sailed from France to the U.S. and was then transported via truck to INL and received at HFEF. The TN-106 cask, after arrival at INL, is shown in Figure 6. Postirradiation examination of FUTURIX-FTA was initiated mid-year in 2015.

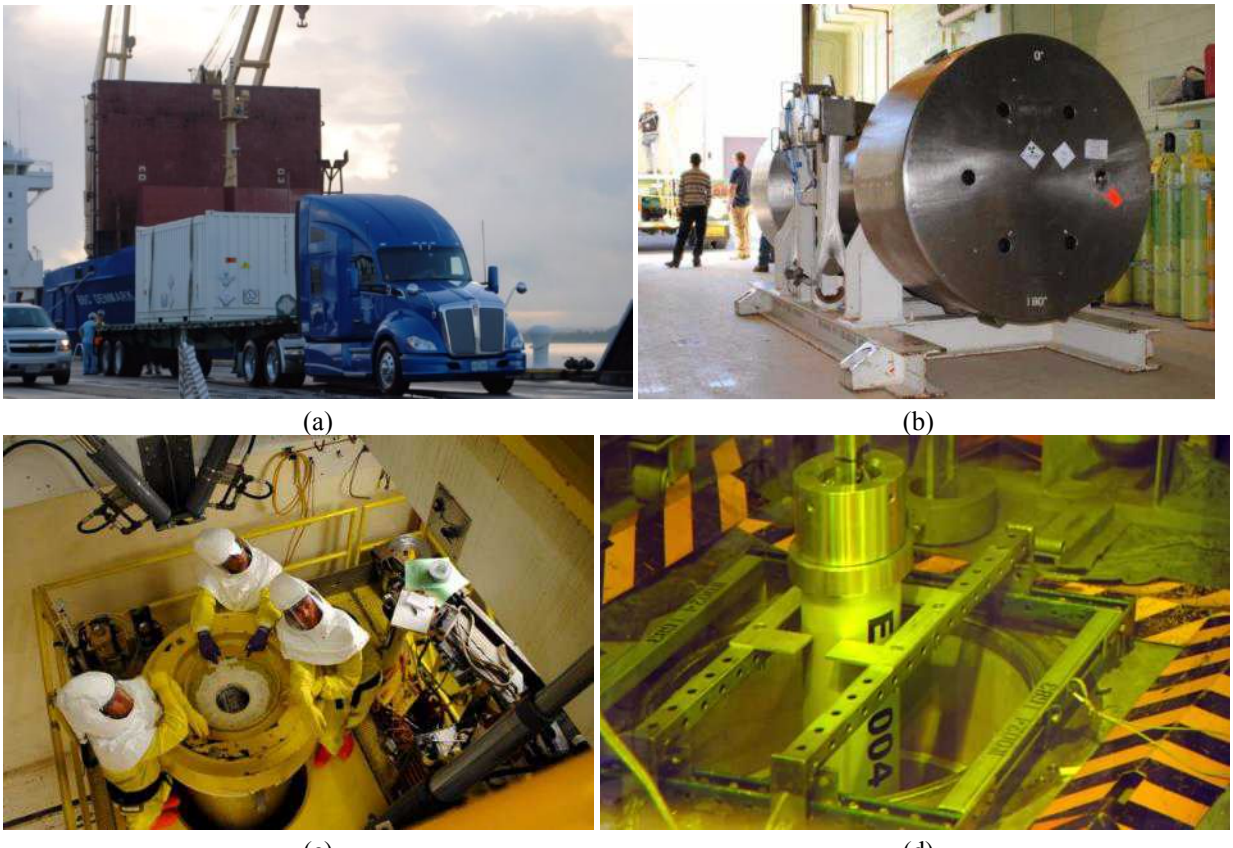

(a) (b)

(c) (d)

Figure 6. Receipt of the TN-106 cask containing the FUTURIX-FTA rodlets (a) at dock in South Carolina (b) in HFEF truck lock (c) in the HFEF cask transfer tunnel (d) unloading the cask into the hot-cell

3. Non-Destructive Examination

A series of non-destructive examinations were performed on the FUTURIX-FTA rodlets after receipt in the HFEF hot-cell. These exams included visual examination, neutron radiography, gamma spectrometry scans, and inspection for changes in dimension. These exams are designed to generally evaluate fuel performance and highlight and areas of the fuel that need to be examined in further detail.

3.1 Visual Exams

Visual examinations were performed through the hot-cell windows. Observations by the hot-cell staff were used to positively identify the elements after removal from the shipping cask by the identification numbers located on the extensions. Nothing unusual was observed on the pins during visual examination. End fittings were placed on the pins to facilitate handling in the hot-cell and increase their compatibility with different hot-cell equipment. The as received state was recorded utilizing through window digital photography. The collected images are shown in Appendix A. There are no obvious visual defects apparent in the rodlets. It is possible to see the transitions between extensions and rodlets in the images.

3.2 Neutron Radiography

Neutron radiography is performed using the neutron radiography reactor (NRAD) located in the basement of HFEF. The NRAD reactor is a 250kW TRIGA reactor with two beam lines. The east beam line services a position below the main floor of the hot-cell and is used for irradiated fuel and the north beam line is being redeveloped for future examination techniques. Neutrons pass through the specimen and expose different activation foils. The radiography fixture contains a scale marked with Gd paint that produces a scale for quantitative measurements of fuel stack dimensional changes. Neutron radiography shots were taken of the FUTURIX-FTA pins at 2 angles with both a Dy foil for thermal neutron radiography and a Cd-covered In foil for epithermal neutron radiography. An

example of the thermal neutron radiography with each pin labeled and demonstrating the spacing of the pins is shown in Figure 7. Detailed neutron radiograms of the fuel material are shown in Figure 8 for thermal neutron radiography and Figure 9 for epithermal neutron radiography. The complete set of neutron radiography can be found in Appendix B.

In the metallic fuel pins the fuel has begun to creep down into the endplugs, but there is no evidence of lift-off. The Na above the fuel appears to be free of any dissolved fuel material. It is possible to see some gaps between fuel

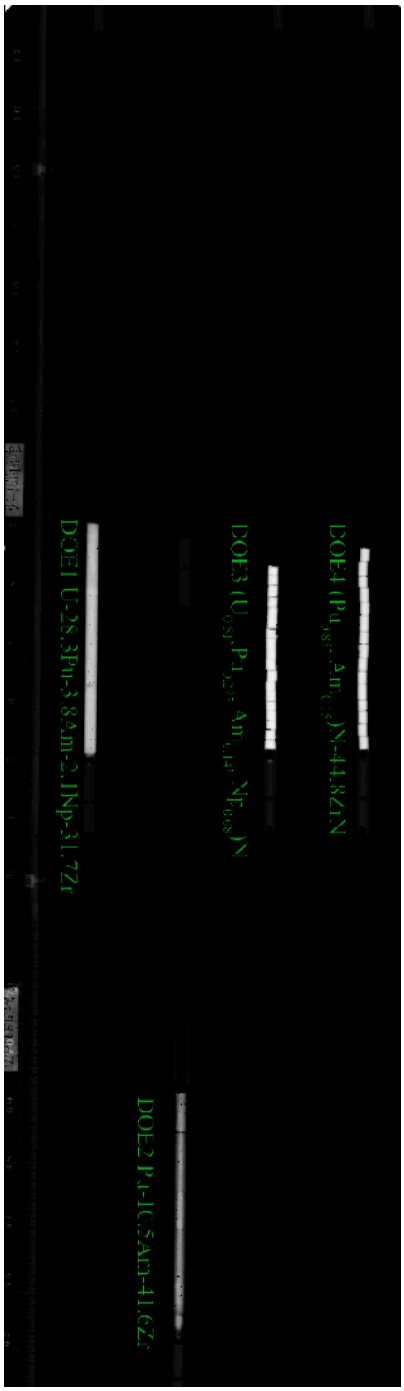

Figure 7. Thermal neutron radiograph showing vertical spacing of FUTUTRIX-FTA fuel stack

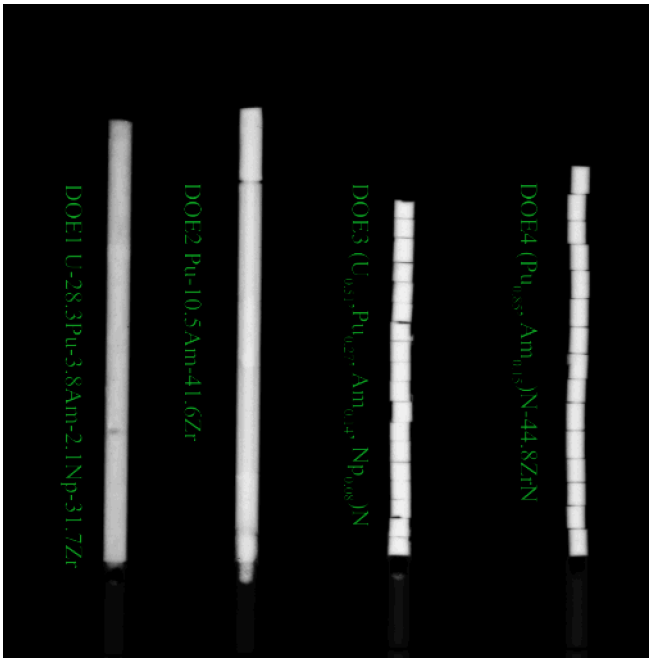

Figure 8. Thermal neutron radiography fuel material detail

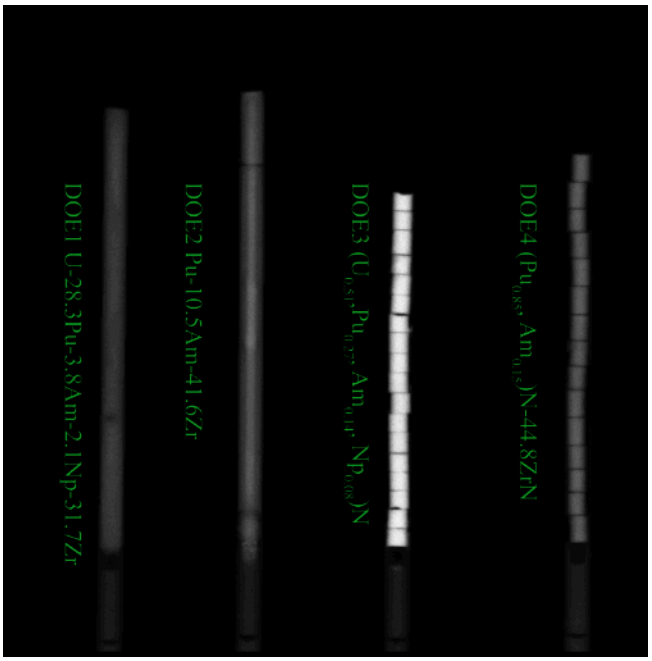

Figure 9. Epithermal neutron radiography fuel material detail

slugs that generally correspond to the original fuel slug dimensions. There is some enhanced neutron attenuation in the epithermal image in the central region of DOE2 that may indicate some constituent (alloying or actinide element) redistribution has occurred. The neutron radiography of the nitride pellets reveals the pellets maintained their geometry fairly well during irradiations and overall appear to have performed well. Some chips can be observed in the neutron radiography, but these chips are all assumed to be artifacts from fabrication. The performance of this nitride fuel is better than some identical nitride fuel irradiated in ATR (AFC-1Æ and AFC-1G). It should be noted that the neutron radiography of AFC-1Æ rodlets 1, 4 and 6 (non-fertile nitride) look similar to the radiography of FUTURIX-FTA DOE 3 and DOE 4 [1, 2].

3.3 Gamma Spectrometry

Gamma spectrometry of all of the rodlets was performed using the HFEF Precision Gamma Scanner (PGS). The PGS has three major components: collimator, stage, and detector. The collimator penetrates the HFEF cell wall with a rectangular aperture that is adjustable form 0.254 cm to 0.00254 cm in height and is 2.2225 cm wide. The collimator can be rotated from a horizontal to vertical orientation. The stage manipulates the sample in front of the collimator in the plane facing the collimator and can rotate the sample about its central axis. The detector consists of a Compton suppressed High Purity Germanium (HPGe) detector and its control system moves the stage and collimator and initiates scans.

Gamma spectrometry was performed on each rodlet individually. The plenum portion of the rodlet was scanned in 0.254 cm steps, and the fueled section of each rodlet was scanned in 0.127 cm steps for a live time of 30 minutes. A strong gamma-ray signal was also detected from Cm-243 which is likely due to the significant Am content in the fuel initially. Further investigation is underway to better understand how to best utilize this signal as it may be possible to ascertain information about Cm and Am distribution in the fuel. A representative gamma-ray spectrum from DOE1 is shown in Figure 10. In this figure, the Cm-243 signal is highlighted in detail. Several fission products were also detected in the gamma spectrometry including: Ru-106 (as Rh-106), Sb-125, Cs-134, Cs-137, Ce-144, Eu-154, and Ce-144 (as Pr-144). Additionally, several activation products including Co-60 and Mn-54. The Mn-54 signal is used in the axial profile plots to show the location of the cladding and cladding endcaps where this signal spikes.

In the metallic fuel (DOE1 and DOE2), Cs radioisotopes have been dissolved in the Na bond between the fuel and the cladding producing a Cs activity spike in the Na plug region above the fuel. This can be seen in Figure 11 and Figure 12. The presence of Cs in the sodium plug is a good indication of rodlet integrity. There are also Cs spikes present at the interface between different slugs used to create the DOE2 fuel stack. This is highlighted in Figure 12 with image overlays of the neutron radiography and the as fabricated fuel slugs lining up with the Cs signal spikes at 89, 92 and 96 cm. Europium has also migrated into the Na bond and plug but is not shown in the figures. There is no evidence of significant rare earth (Ce) migration to the fuel periphery which might indicate unexpectedly high levels of fuel cladding chemical interaction. The relative level of Ce migration to the fuel periphery is measured by comparing the Ce-144 activity calculated by the 133.5 keV gamma-ray and the higher energy (696, 1489 and 2186 keV) gamma-rays from the daughter of Ce-144, Pr-144, that is in secular equilibrium with Ce-144. The Ru in these rodlets appears to be well integrated into the fuel as does the Cm-243. Both of these signals are plotted in Figure 11 and have a similar shape for DOE2.

The gamma spectrometry of the nitride rodelts (DOE3, and DOE4) reveals Cs migrating out of the fuel and depositing in the cooler sodium plenum as predicted by thermodynamics. This is seen as small shoulders on the Cs distributions shown in Figure 13 and Figure 14. All other fission products appear to have been retained in the fuel matrix. The Cm-243 signal in DOE4 was significantly lower than expected based on the nominal composition and the Cm-243 signal from DOE3. However, the atomic density of Am is higher in DOE3 than DOE4 as-fabricated, so the Cm-243 signals are consistent. The Cm-243 signal contains a great deal of statistical noise in DOE4 and is not plotted in Figure 14. As was the case with the metallic fuel, the Ru signal for the nitride fuels indicates that it and likely other noble metals (Ru, Rh, Pd, Mo, Tc) are stable in the fuel matrix.

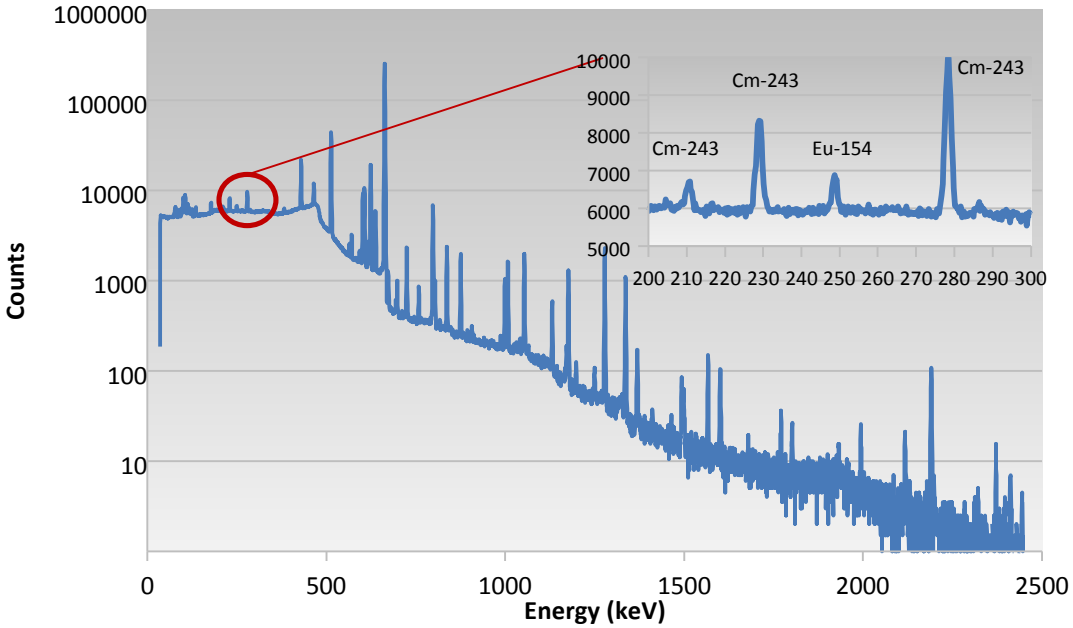

Figure 10. Representative gamma-ray spectrum from DOE1 (U-29Pu-4Am-2Np-30Zr) Fuel Centerline with a detail of the spectrum corresponding to the Cm-243 signal

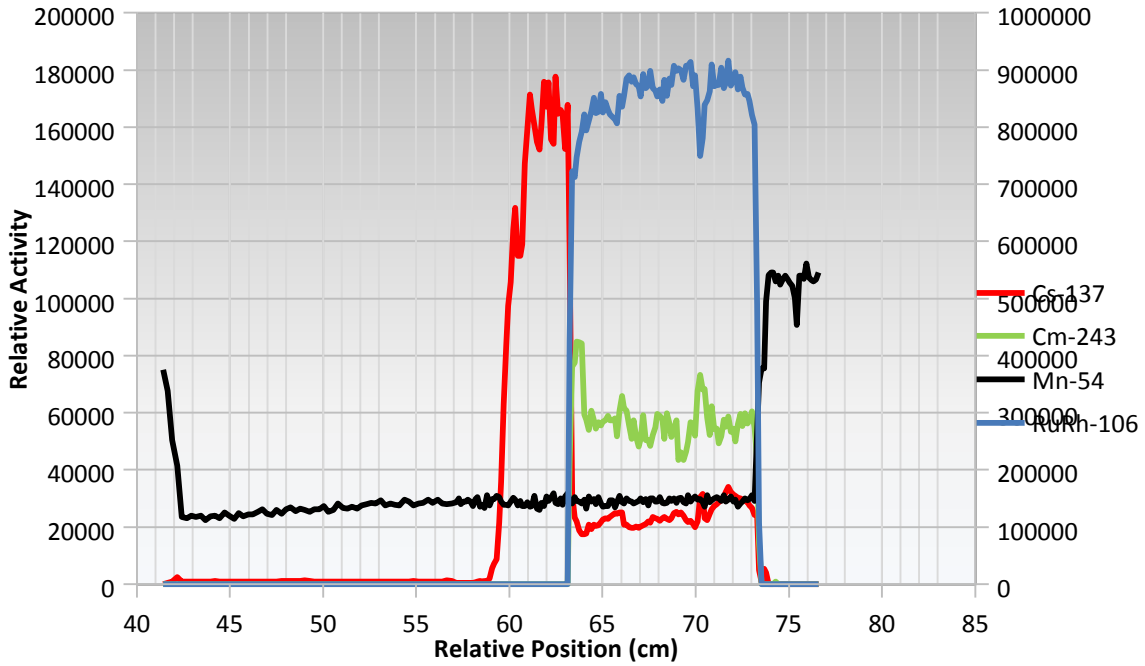

Figure 11. Fission Product Distribution in DOE1

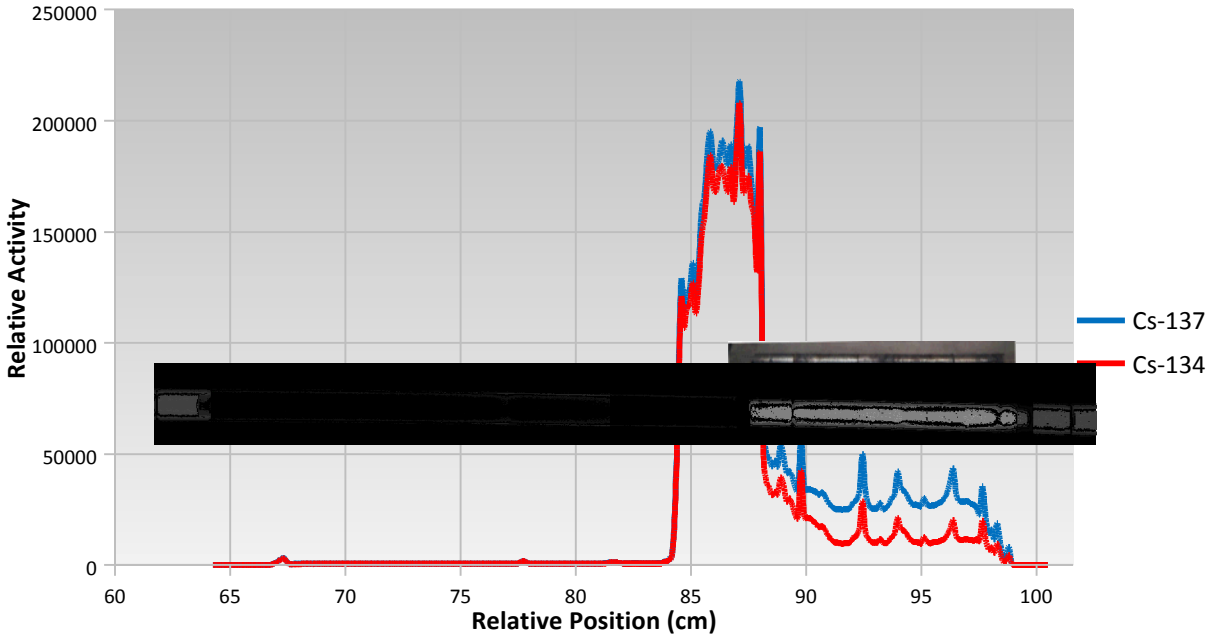

Figure 12. Cs Distribution in DOE2

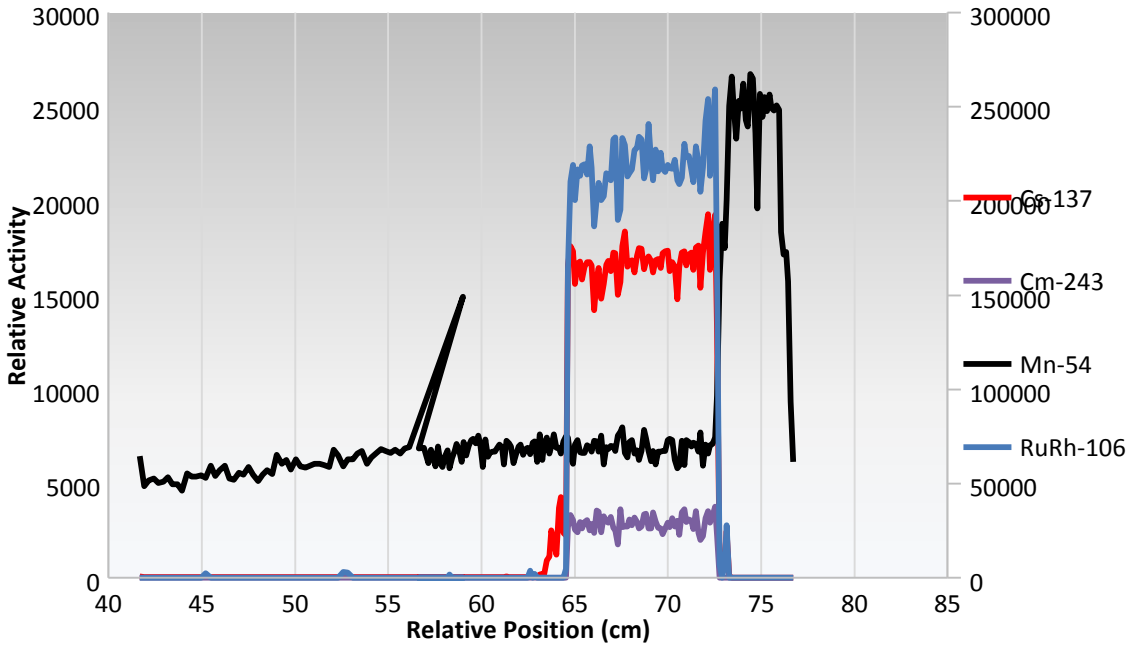

Figure 13. DOE3 Fission Product Distribution

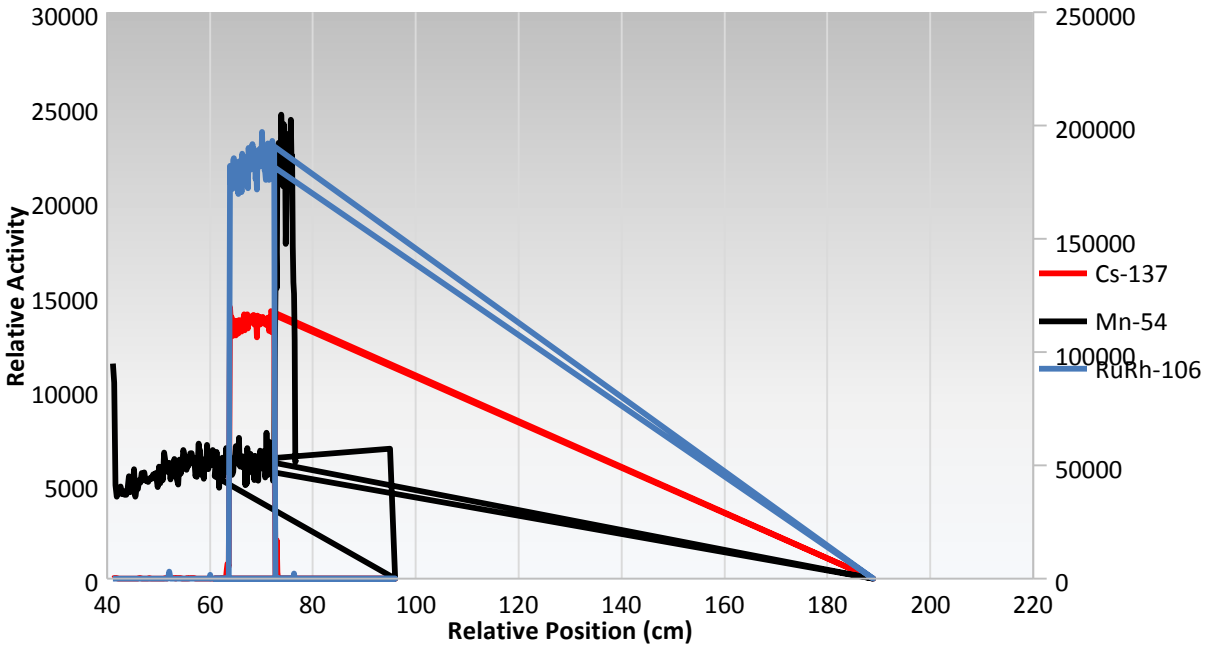

Figure 14. DOE4 Fission Product Distribution

In addition to axial gamma spectrometry scans, it is possible to rotate the HFEF PGS collimator from a horizontal to a vertical orientation. In this orientation it is possible to move an axial level of the fuel past the collimator and then perform a series of rotations over several angles. The resulting signals over several angles can be collected and tomographically reconstructed to produce a two dimensional distribution of fission products averaged over an axial location. This is referred to as Gamma Emission Computed Tomography (GECT). The full details of this technique are available in Reference 17 and the demonstration of this technique can be seen in Reference 18 and 19. This technique is similar to conventional X-ray computed tomography, but it is limited by the number of angles that can practicably be collected as each step spectrum collection takes several minutes and the total collection time can take several days.

The GECT technique was applied to both DOE1 and DOE2 in 0.0254 cm steps over 16 equally spaced angles between 0 and 180°. For both rodlets, data was collected at the mid plane of the fuel slug. The results of the GECT for Cs-137, Ru-106, and Cm-243 are shown in the Figure 15, Figure 16, and Figure 17 respectively for both DOE1 and DOE2. The Cs-137 distribution is quite different for the two rodlets shown in Figure 15. Optical microscopy sheds some light on this behavior and is discussed in Section 4.2. In short, there was a great deal of open porosity in the interior of the DOE1 fuel pin at this level. Cs produced by fission likely was dissolved in Na that migrated into the open porosity in this region of the fuel. In the past, a similar Cs spike was also observed in the interior fuel. During the IFR program, a punch EDM was used to look at several radial positions in irradiated U-20Pu-10Zr fuel. When the samples were counted, the Cs profile matched the distribution seen in Figure 15(a). However at the time, this result was not believed and was not published [20]. Further investigation into this behavior might be warranted as this behavior might have implications on how the fuel is modeled in thermal simulations. The Cs distribution in DOE2 appears to be in a ring around the fuel slug. This is the behavior typically seen in other metallic fuel [19]. This likely indicates Cs has migrated to Na that is still largely residing between the fuel and the cladding. The distribution of Ru-106 for both DOE1 and DOE2 are similar and shown in Figure 16. The distribution is a ring, but the axially data suggests Ru-106 is stable in the fuel. The ring of Ru may indicate where the majority of the fission reactions were occurring. The lack of Ru-106 and by implication fission in the center may indicate Zr redistribution in the fuel which is likely for DOE2. For DOE1, it may also be indicative of the open porosity forming in DOE1 that was indicated by the Cs signal. Alternatively, the ring or Ru may be an indication of mobility above a certain temperature where the Ru is moving out of the hot central region of the fuel into the cooler periphery of the fuel. The Cm-243 signal is shown in Figure 17, and this result is also hard to interpret. The signal strength from DOE1 is not excellent, but generally appears to be a fairly constant distribution across the fuel. The signal from DOE2 indicates a ring where no Cm-243 is located. This may suggest some chemical migration in the fuel that has shifted

the Am or Cm concentration away from the mid-radius of the fuel. Future electron probe micro-analyzer (EPMA) work will likely be needed to confirm this observation. Understanding of this observation will likely require some additional chemical modelling of this complex actinide and Zr system.

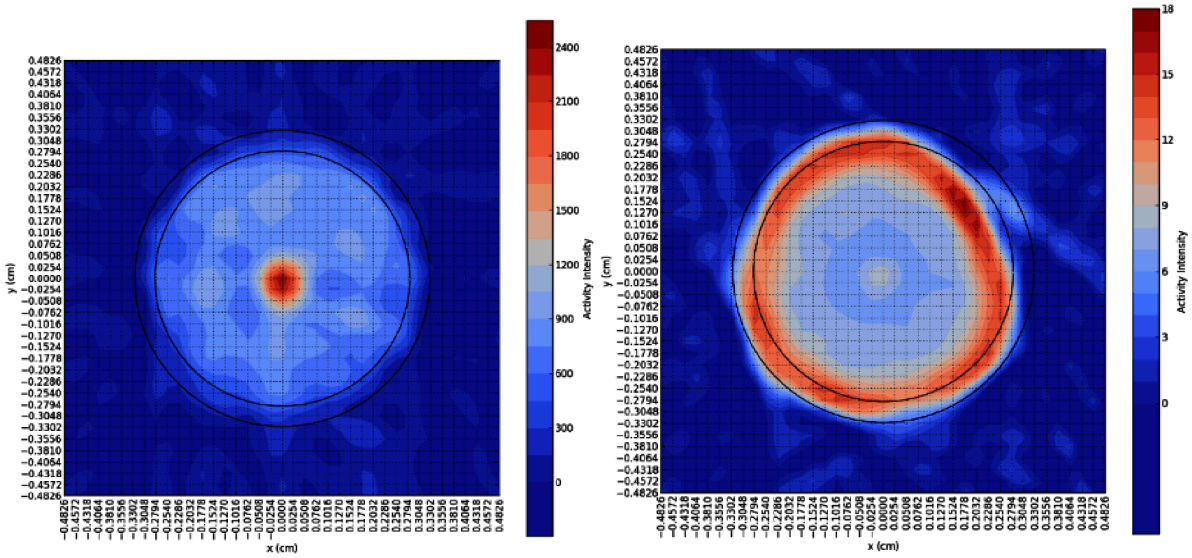

(a) (b)

Figure 15. Cs-137 Distribution in the middle of the fuel zone for DOE1 (a) and DOE2 (b)

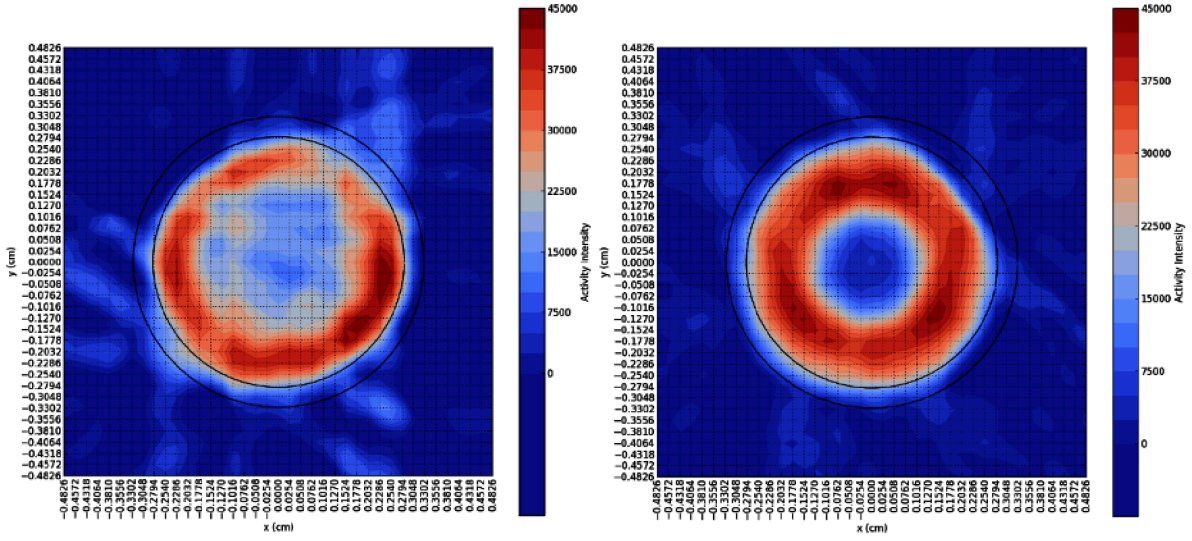

(a) (b)

Figure 16. Ru-106 Distribution in the middle of the fuel zone for DOE1 (a) and DOE2 (b)

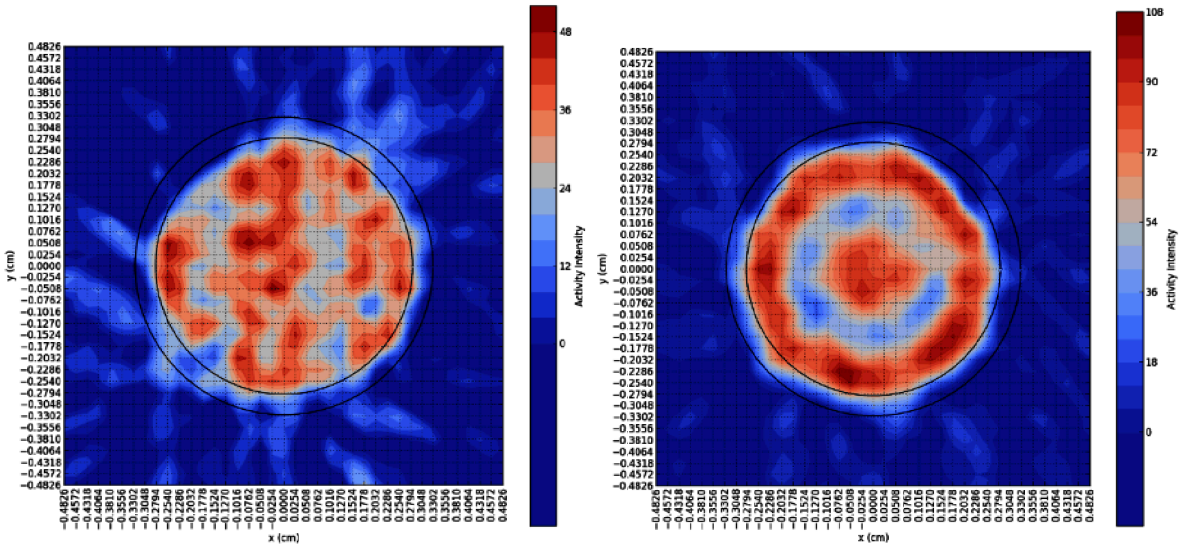

(a) (b)

Figure 17. Cm-243 Distribution in the middle of the fuel zone for DOE1 (a) and DOE2 (b)

3.4 Dimensional Inspection

Dimensional inspection was performed with the HFEF element contact profilometer. Diameter measurements were collected all along the pins in roughly 0.127 cm increments and at 6 angles spaced 30° apart. Diameter measurements are collected with ±0.0005 cm accuracy. The diameter measurements were performed prior to the removal of the extensions and it is possible to ascertain the beginning and end of the rodlets by diameter spikes caused by welding on the extensions and rodlet endcaps. Given the accuracy of the instrument no perceptible strain was detected in any of the 4 pins. In the metallic fuel pins where fuel was present, there may have been a diametral strain of 0.1%, but this strain is at the limit of the instrument uncertainty. Diametral strain was calculated based on the as-fabricated diameter of the AIM-1 cladding which is 6.565 mm. The measured diametral strain is shown in Figure 18, Figure 19, Figure 20, and Figure 21 for DOE1, DOE2, DOE3, and DOE4 respectively. The jumps in stain indicate the locations of welds where the rodlets are attached to endcaps and extensions. The rodlets are shown plenum to the left and fuel zone to the right. The uncertainty shown for each measurement is 7.7×10^{-4}, which is the 1 sigma uncertainty. Thus while there is a consistent strain indicated in the fuel zone of DOE1 and DOE2. This strain is at the limit of the sensitivity of the HFEF element contact profilometer.

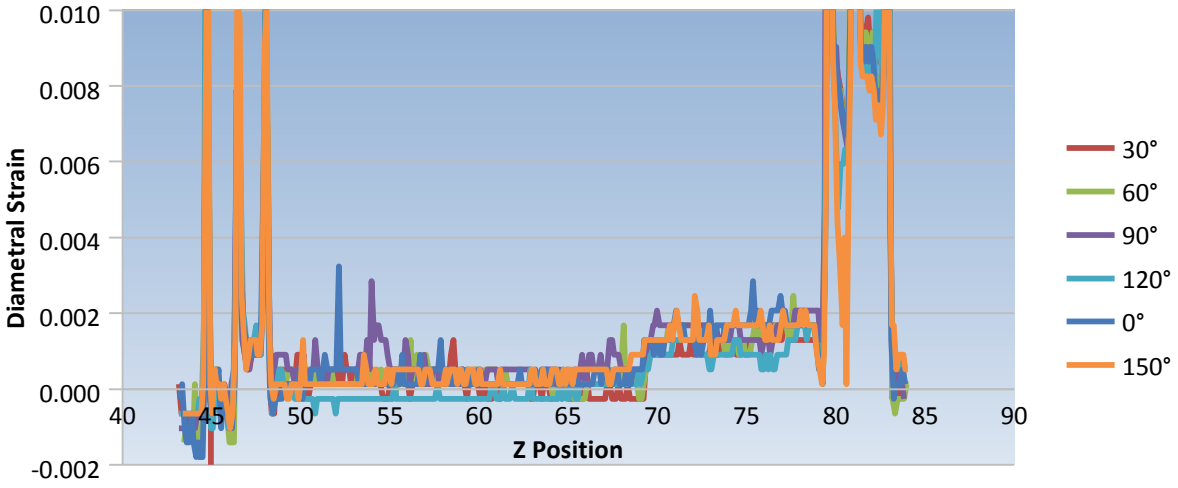

Figure 18. Diametral strain measured for DOE1

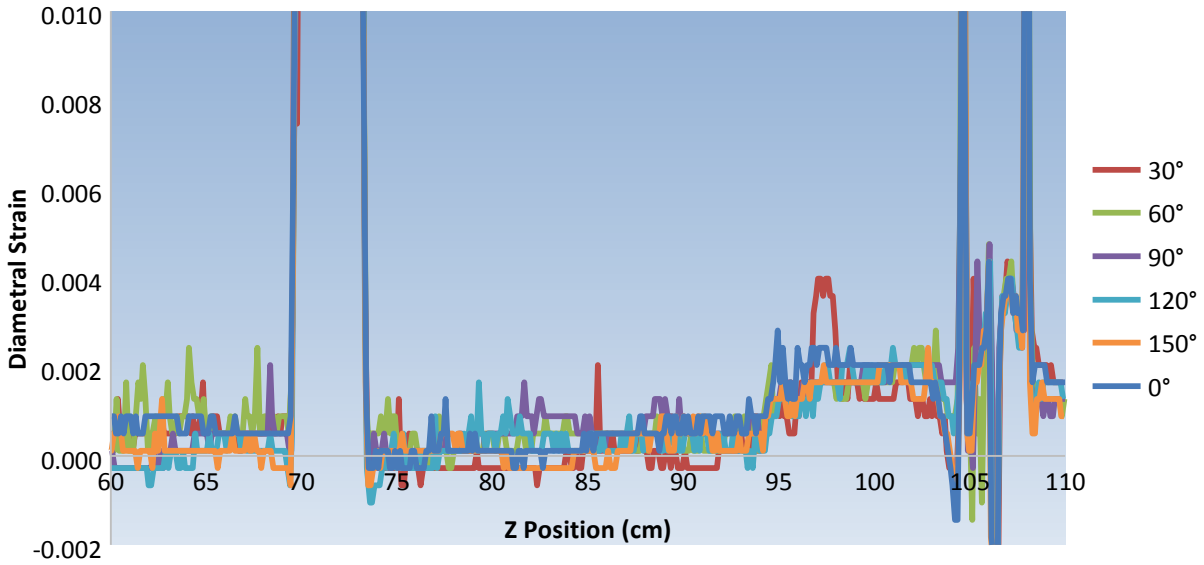

Figure 19. Diametral strain measured for DOE2

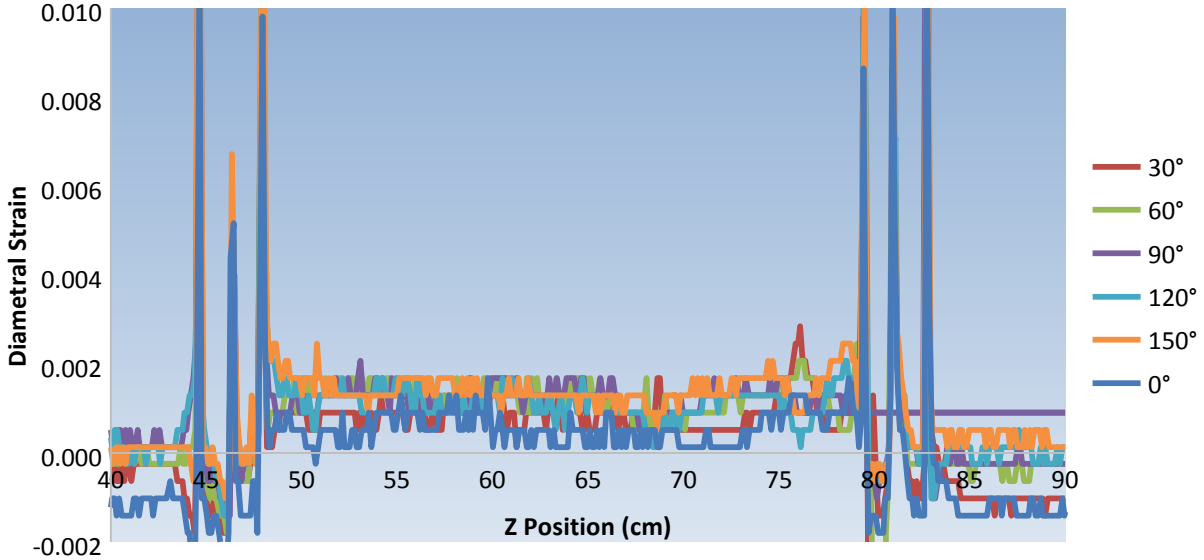

Figure 20. Diametral strain measured for DOE3

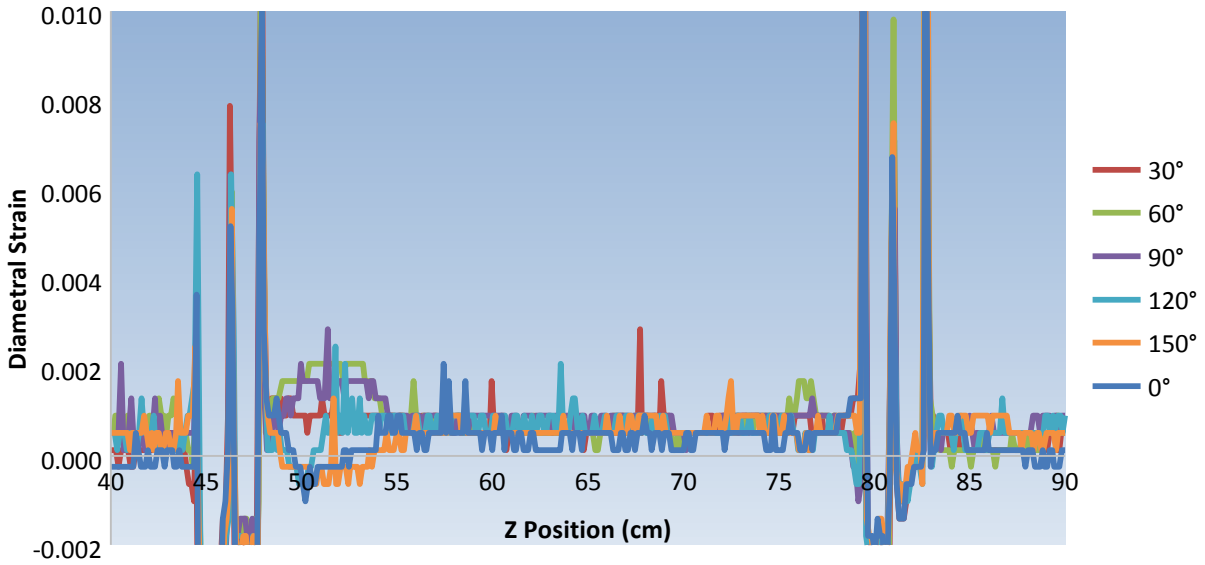

Figure 21. Diametral strain measured for DOE4

4. Destructive Examinations

At the conclusion of the final NDE exams, destructive examination was carried out on the FUTURIX-FTA rodlets. Destructive examination is considered to start when the fuel pins are punctured for fission gas release analysis. Baseline destructive exams include fission gas release analysis, optical microscopy, and analytical chemistry analysis for burnup. Microhardness was not performed on FUTURIX-FTA samples. The value of microhardness data is primarily in the cladding and confirming FCCI layers. There was no prominent FCCI observed in the optical samples. Additionally, the AIM1 cladding used in this experiment is not a cladding of interest for future irradiations negating the need to investigate irradiation induced changes in the material.

4.1 Fission Gas Release

Fission gases were collected from the rodlets using the HFEF Gas Assay, Sample, and Recharge (GASR) system. Rodlets were punctured using a 150 W Nd-YAG laser system and a gas sample was collected in a stainless steel bottle external to the hot cell. Void volume in the rodlet was then determined by a series of backfills into the punctured rodlet and expansions into the GASR system. The fuel rodlet internal gas pressure was derived from the void volume measurement and the initial gas pressure measurement upon puncture. Fission gas analysis was performed by gas mass spectrometry at Pacific Northwest National Laboratory (PNNL). Results of fission gas analysis provided total elemental composition and krypton and xenon isotopic composition. A summary of results is shown in Table 4. The combined Kr and Xe release is based on an estimate of the number of fissions that occurred in each rodlet from U-235 and Pu-239 and an empirical relationship between fission and atoms of Xe and Kr produced. The number of fissions in each rodlet was determined from ICP-MS results discussed in Section 4.3. All fission was assumed to have come from Pu-239 in this calculation. The production of Kr and Xe is based on the fast fission yields of the stable Kr and Xe isotopes.

There was a significant amount of Ar in the plenum and it was important to establish if this gas was from the original welding of the plenum or from contamination from the hot-cell. The FUTURIX-FTA rodlets were welded in a 75% Ar, 25% He gas mixture [21]. The total number of moles of gas present in the plenum can be calculated from the plenum pressure and the plenum volume using the ideal gas law. The PIE amount of Ar was compared to the expected amount of Ar in the pin from welding, and the two values were found to agree within less than 4%.

The resulting fission gas releases are reasonable. The metallic fuel fission gas release is close to the 70%±10% fission gas release that is expected from typical 75% smeared density U-Pu-Zr fuel behavior beyond 5 atom % burnup after porosity interconnects [22]. The release value for DOE 1 is a little low compared to literature, but some of the AFC-1H pins with similar compositions and fission densities also had Kr+Xe releases between 50 and 60% [2]. The DOE2 fission gas release is exactly in line with historic expectations of metal fuels. The nitride fuel fission gas release is very low which is expected from the very short irradiation the nitride fuels saw. The helium

release was 62 and 64% for the metallic fuel and 3 to 6 % for the nitride fuels. This release is primarily from the α decay of the minor actinides present in this fuel and must be considered in high burnup high minor actinide bearing fuel pins due to its impact on plenum pressure. This release seems reasonable when compared to the results from AFC-1. There is not a large historical data base for He release from minor actinide bearing fuels.

Table 4. Fission Gas Release Summary

Rodlet	Plenum Pressure (MPa)	Plenum Volume (cm^3)	Gas Composition – Major Components (%)						Kr+Xe Gas Release (%)	He Gas Release (%)
			He	N	O	Ar	Kr	Xe		
DOE1	6.28E-01	4.453	19.987	0.025	0.002	10.734	4.704	64.505	51.6%	62.4%
DOE2	9.20E-01	4.422	29.349	0.009	0.030	7.265	4.169	59.099	69.3%	64.2%
DOE3	9.86E-02	5.491	29.985	0.010	<0.001	65.668	0.344	3.924	3.4%	3.4%
DOE4	9.38E-02	5.524	28.896	1.145	0.123	66.848	0.225	2.578	2.5%	6.6%

4.2 Optical Microscopy

Optical microscopy was performed on fuel cross sections to investigate irradiation induced features in the fuel microstructure. The extensions were cut 25.5 inches below the end fitting and 9 inched below the end fitting to free the DOE 1, 3 and 4 rodlets. The DOE2 rodlet was separated from the extensions by cutting 35.5 inches and 19 inches below the end fitting. These cuts were designated to be 1 inch away from the outer weld that held the extensions to the rodlet endcaps. The extensions were archived to the Nuclear Science Users Facility (NSUF) Sample Library for future exams by an interested party. Neutron radiography and the visual exams were used to guide the sectioning of the fuel in the approximate center of the fuel column. Sectioning was achieved using a low speed saw with a diamond coated wafering blade. A 5.0 mm slice of fuel was cut for analysis at the Analytical Laboratory and another 5.0 mm slice of fuel was mounted for grinding and polishing. The slices were mounted in INL IMCL EPMA compatible rings with an outer diameter of 25.146± 0.0762 mm (0.990±0.003 inches). The sectioned fuel was placed in the met mount and back filled with epoxy that contained approximately 15 wt.% graphite for conductivity. This was done to facilitate electron microscopy in future examinations. Grinding was achieved using 400 grit grinding plates followed by 800 and 1200 grit plates. Polishing was achieved using 6, 3, 1, and 0.25 µm diamond suspension. This produces a surface that is more than satisfactory for optical microscopy. Grinding and polishing were performed in the HFEF Containment Box (Window 2M). After polishing samples were transferred to the HFEF Met Box (Ar atmosphere) for examination on a Leitz MM5RT metallograph. Images were recorded with an integrated digital camera. Montages of the fuel cross sections were assembled from 50X images. Montages of scans across fuel cross sections were captured at both 100X and 200X. The light source was polarized during image collection, and images were captured in 8-bit color. Higher magnification images were recorded of features of interest. All the major observed features of the fuel are discussed in this section. Higher resolution images are available and the complete set of microscopy has been uploaded to a shared AFC PIE network drive (\\Fn2\projects\AFC ATF PIE Dat\FUTURIS-FTA) (only available on the INL network by request).

A few important historic fuel performance criteria are worth noting when interpreting the observed microstructure. This review is focused on metallic fuel due to the limited data set available for nitride fuels. There have only been about 200 nitride pin irradiated in fast reactors [9]. Also, the limited irradiation that the FUTURIX-FTA nitride fuels saw limits the irradiation induced changes that are possible in the samples. Ideally the metallic fuel irradiated in FUTURIX-FTA would behave in a manner that is consistent with the well-established historic behavior of U-5Fs, U-10Zr and U-20Pu-10Zr fuel that was irradiated in EBR-II and other fast reactors. Likewise the nitride fuel in FUTURIX would ideally behave as nitride fuels have behaved in historic irradiation campaigns also performed in EBR-II and other fast reactors. The difference between the FUTURIX-FTA fuel and historic fuel forms is the large amount of minor actinides present in the fuel. If fuel performance is not degraded by significant

quantities of minor actinides in the fuel matrix, these isotopes can be effectively destroyed in fast spectrum reactors.

During the development of metallic fuel, 75% smear density was found to be the optimum compromise between fuel loading and fuel swelling in metallic fast reactors. Obviously fuel loading should be maximized to maximize cycle length or actinide destruction in a fast reactor. At 75% smear density, as metallic fuel swells with fission gas production, the porosity will interconnect releasing fission gas to the plenum without placing excessive strain on the cladding. However at high burnup solid fission products begin to fill the voids and again begin to put strain on the cladding. Lower smear density fuels are then necessary to push fuel performance to high burnup beyond 15 at.% (%FIMA). Alloying elements added to U serve two purposes: to raise the melting temperature and to help stabilize the cubic phase of U (γU) or U and Pu. Zirconium at 10 wt.% of the fuel historically worked very well for this purpose, but it does undergo constituent redistribution during irradiation. In U-10Zr, the Zr migrates to the center of the fuel pin. This raises the melting temperature in the center of the pin where the temperature is hottest during steady state irradiation, but this phenomenon lowers the melting temperature in the fuel periphery which may be problematic in certain transient accidents. In ternary fuels with U-Pu-10Zr, the Zr concentrates in both the center of the fuel pin and at the pin periphery. In both cases, the U depletes when the Zr concentrates, but Pu concentrations do not vary in ternary fuels under irradiation [4, 5, 7, 8]. If this behavior changes with the addition of Np and Am to the fuel is an important point of investigation for FUTURIX-FTA PIE. Beyond baseline examinations will need to be performed to fully understand the consequence of minor actinide addition to the fuel

Fuel cladding chemical interaction (FCCI) in metallic fuel has also been studied in detail. Metallic interdiffusion drives FCCI in metallic fuels however the rate of interaction varies widely based on the interplay of all the major alloying elements present in the system and some of the minor constituents as well. Early work showed Ni accelerated interdiffusion which is one of the drivers to move from 300 series stainless steels to ferritic-martensitic steels. The majority of French experience is with oxide fuels for fast reactors which are more compatible with austenitic steels. FUTURIX-FTA was clad using the austenitic AIM1 alloy to facilitate irradiation in Phénix, but any metallic fuel irradiation would ideally occur in a martensitic steel. The presence of lanthanide fission products, either from high burnup or carry over from fuel reprocessing, can enhance FCCI. Historically the addition of Zr to the U fuel was important in impeding FCCI. The eutectic temperature of U and Fe at 719°C is one important mechanism in metallic fuel FCCI, but other elements present at the fuel cladding interface impact the thermodynamics and kinetics of this eutectic point. Other elements such as the rare earths in U-Zr alloy fuels may also have low temperature eutectic reactions that are equally important to the rate of interdiffusion driving FCCI [4, 5, 7, 8].

The cross section for DOE1 MNT-20Y (U-28.3Pu-3.8Am-2.1Np-31.7Zr) was prepared twice. The surface revealed by the initial preparation is seen in Figure 22 and in greater detail in Figure 24 and the surface revealed by the second preparation is seen in Figure 23 and in greater detail in Figure 25. The first preparation revealed a surface where the central region was highly porous. It was assumed that some of the highly porous structure fell out during sample preparation resulting in the large black void seen in Figure 22. This void was actually visible through the hot-cell window. With the amount of central porosity seen in Figure 22 and Figure 23, the Cs behavior seen in Figure 11 appears more reasonable. An alternative explanation to the difference in microstructure between the two cross sections is that the void observed in Figure 22 is that an actual pressurized void had formed and all the porosity locally migrated to the center leaving the fuel in the outer radii denser. In contrast the local porosity in Figure 23 is more evenly distributed locally. In both preparations the porosity is spherical in shape throughout most of the fuel. In the second preparation the very outer periphery of the fuel the porosity is smaller and somewhat lenticular. This would tend to indicate that the underlying crystal structure of the fuel material is cubic everywhere except the outer 500μm. However with the amount of porosity present the typical porosity behavior of binary and ternary U-Zr and U-Pu-Zr alloys may not hold. In a binary or ternary metal fuel lenticular pores are formed in fuel

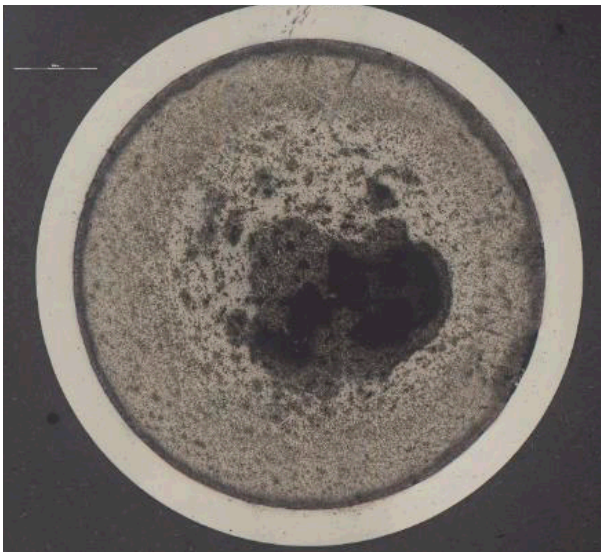

Figure 22. Montage of images collected from first preparation of cross section of DOE1

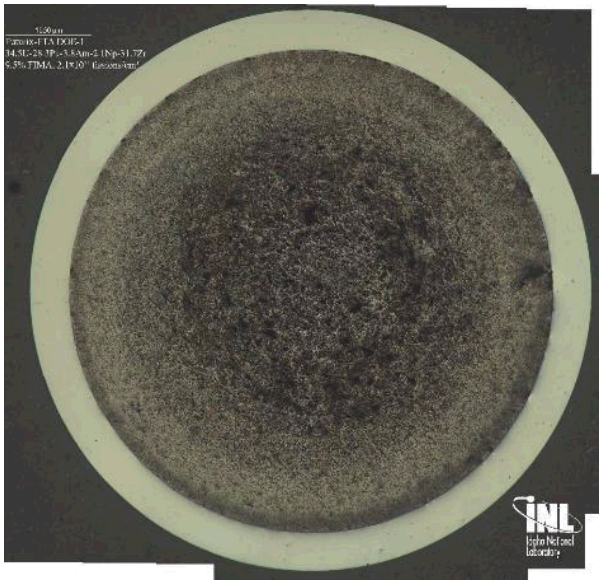

Figure 23. Montage of images collected from second preparation of cross section of DOE1

Figure 24. Higher magnification detail of radial microstructure revealed in first preparation of DOE1

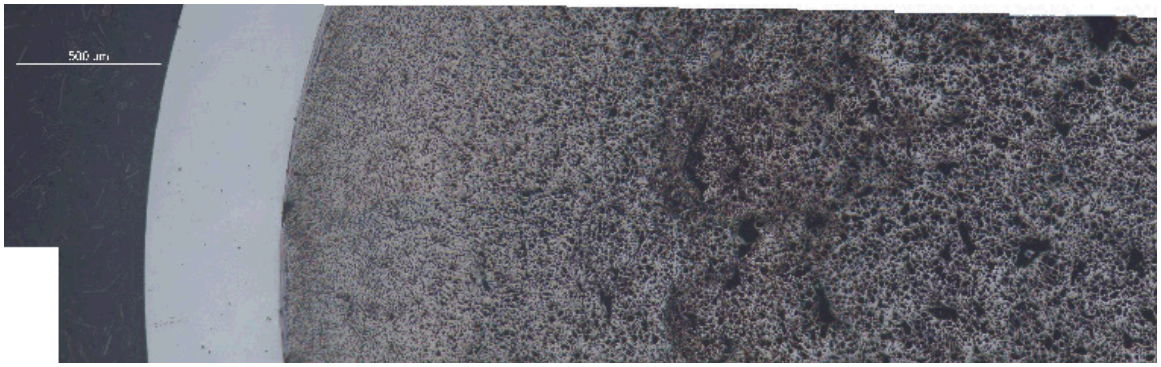

Figure 25. Higher magnification detail of radial microstructure revealed in second preparation of DOE1

The cross section from DOE2 MNT-21Y (Pu-10.5Am-0.3Np-41.6Zr) is shown in increasing detail in Figure 26, Figure 27, and Figure 28. The cladding has several spots with debris and tarnishing from polishing. The black marks on the cladding in Figure 26 should not be mistaken for cladding degradation. This cross section shows evidence of constituent redistribution and phase separation. There are several rings of microstructure present in Figure 26 that suggest different phases that were present during irradiation and these phases are likely driven by different thermal conditions present in the fuel during irradiation. The Pu-Am-Zr system is not as well understood

as the U-Zr or the U-Pu-Zr system, but many of the same observations made on the DOE1 cross section can be made and tied back to know properties of the Pu-Zr system. As-fabricated, XRD of the fuel revealed the predominant microstructure to be δ-(Pu,Zr) [13]. During irradiation the cladding temperature was about 550°C, so it is likely that during irradiation both δ-(Pu,Zr) and ε-(Pu,Zr) were present in the fuel. Both of these phases are cubic and the porosity structure suggests a cubic crystal structure. As in DOE1 there is a ~20μm layer that is likely a Zr rich layer from fabrication, or it could be a FCCI interaction layer. There are at least 5 major zones of microstructure in the fuel. The first three from the outer radius of the fuel inward about 1mm all have small porosity and varying amounts of what appears to be phase separation supposed by different colors in the microscopy which often indicates various different levels of oxidation. Certain layers oxidize faster than others presenting a different color. In the next 750 μm the porosity of the fuel changes significantly and becomes much larger. The color of the fuel matrix also suggests that this is a more homogeneous phase in the fuel. This is all visible in Figure 26 and Figure 27. The interior of the fuel has a great deal of phase separation. In Figure 27, one of phases is much more susceptible to tarnish and is orange in the collected microscopy. The orange phase tends to cluster and is surrounded by a lighter matrix phase. The matrix phase is shown in detail in Figure 28. If it is assumed that the appearance of the stacked structure is indication of a different chemical phase not a different crystallographic orientation in the material, the matrix phase has a stacked structure that is suggestive of the decomposition of γ(U,Zr) into αU and δUZr_2. The stacked structure in this fuel could be the decomposition of ε-(Pu,Zr) into δ-(Pu,Zr) and αZr. If Zr redistribution did drive additional Zr up the temperature gradient to the center of the fuel this explanation is also more likely. The exact nature of these phases and the location of the Am in the fuel will require further investigation likely with at least an EPMA exam. Micro-XRD and the preparation of transmission (TEM) lamella by Focused Ion Beam (FIB) would also be helpful to fully understand this system.

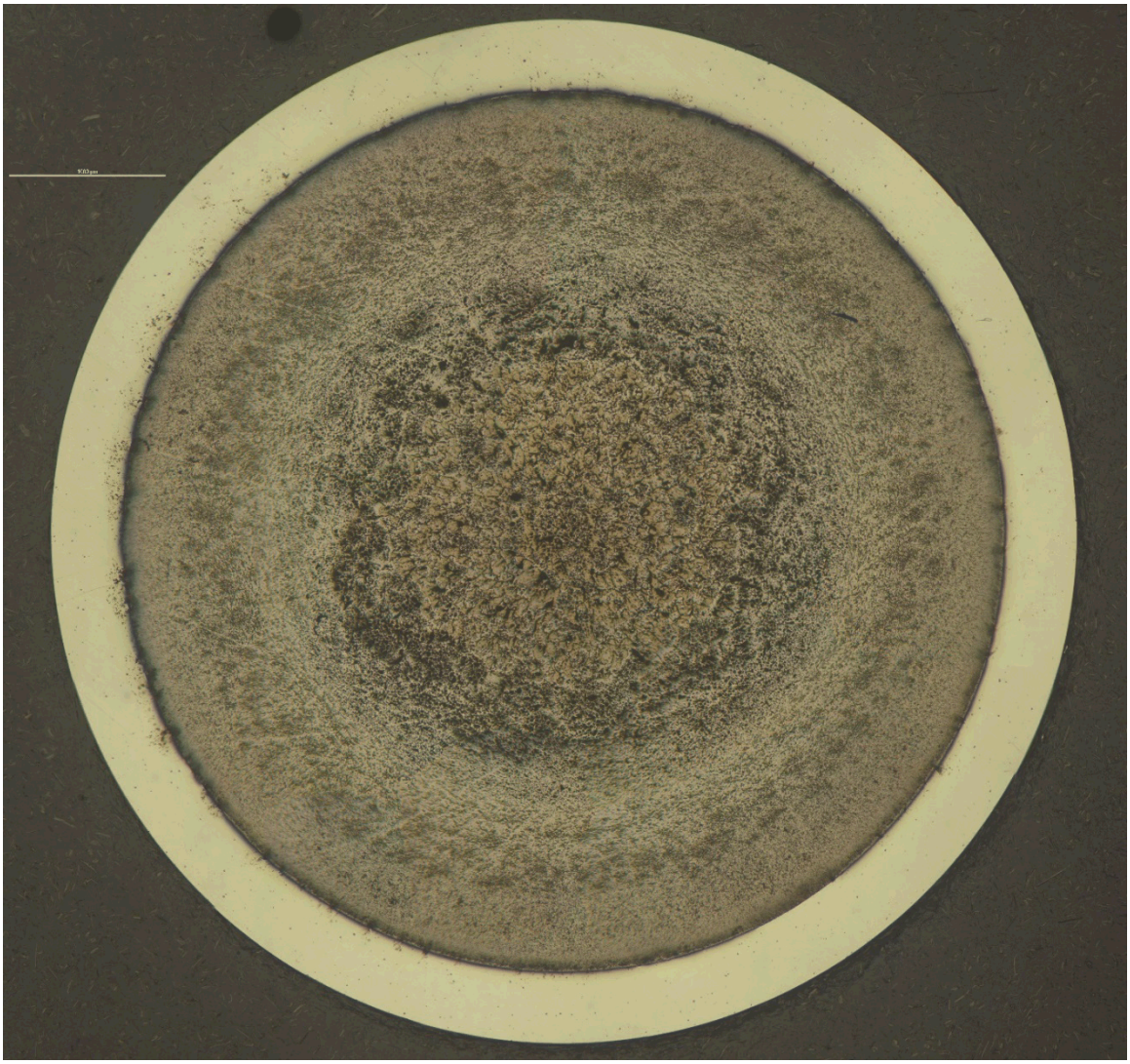

Figure 26. Montage of images collected from cross section of DOE2

Figure 27. Higher magnification detail of radial microstructure revealed in DOE2

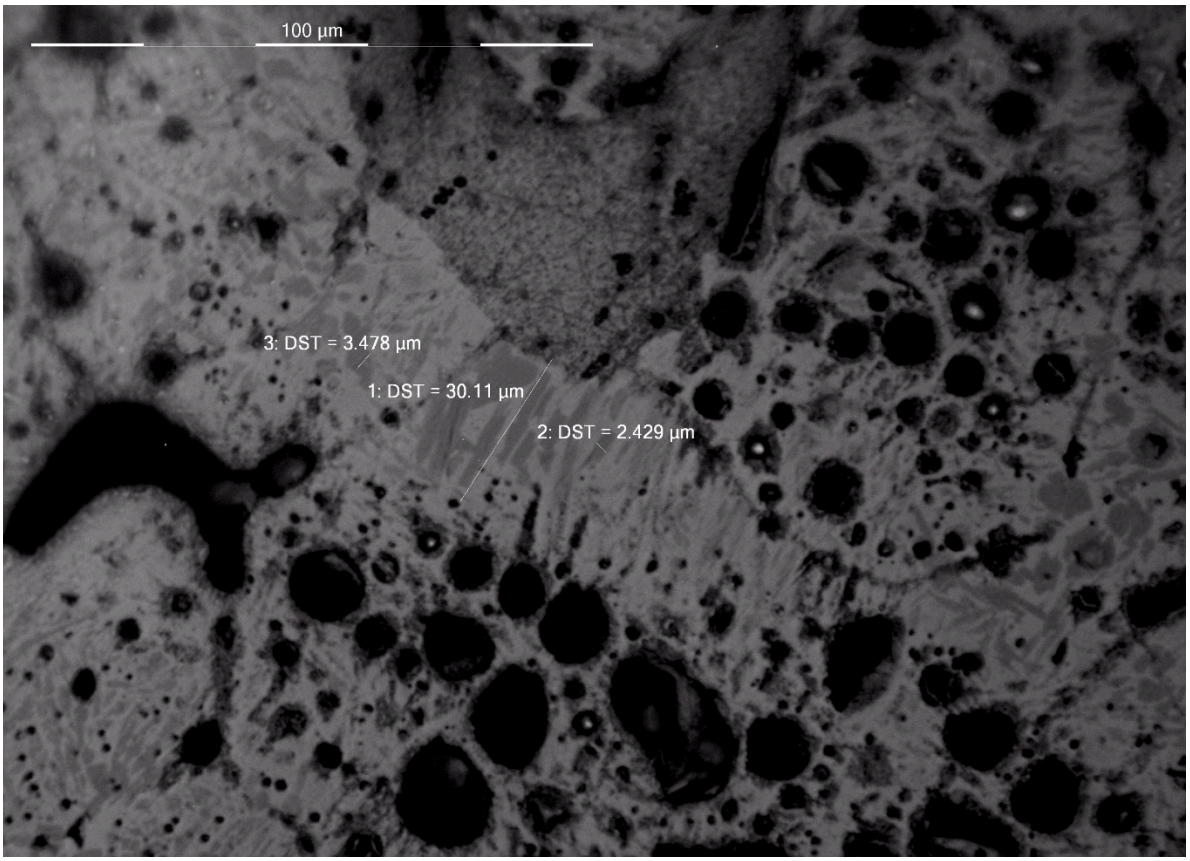

Figure 28. Detail of phase separation present in the central region of DOE2 MNT-21Y

The nitride fuels are more straight forward than the metallic fuels largely due to their lower burnup. Optical microscopy images from the prepared cross section from DOE3 ($(U_{0.51}Pu_{0.27}Am_{0.14}Np_{0.08})N$) are shown in Figure 28 and Figure 29. In Figure 28, there is a large smudge on upper left of the DOE3 cross section that is an artifact from preparation and could not be removed with wiping. The microstructure in Figure 28 and Figure 29 is largely unchanged from the as-fabricated microstructure [14]. This is demonstrated in Figure 31. A similar comparison is shown in Figure 32 for the cross section prepared from DOE4. A higher magnification image of DOE4 is shown in Figure 33. Again this pellet has not changed much from the as-fabricated microstructure. As with the as-fabricated pellets, there is a lighter lower porosity rind on the pellet and a higher porosity center. There are also several areas of large grains interspersed with smaller grained material. There is not consistent evidence of any fission product phases forming in this fuel. With nitride fuel just like with oxide fuel it is possible to create an Ellingham diagram to look at the thermodynamic stability of the fission product nitrides versus the stability of the constituent actinide nitrides. If a higher burnup had been achieved it would have been reasonable to expect noble metal precipitates (Mo, Tc) analogous to what is seen in oxide fuels. Other noble metals (Pd, Ru, Rh) may form intermetallics with the actinides which might be detrimental to long term fuel performance through the creation of low melting phases. At the cladding temperature of 550°C, some rare earths (Pr, Nd, Sm, Ce) will form stable nitrides while others (La, Eu) will not which might cause longer term problems with FCCI. The most thermodynamically stable nitride fission product is ZrN which is also used to stabilize the non-fertile nitride pellets.

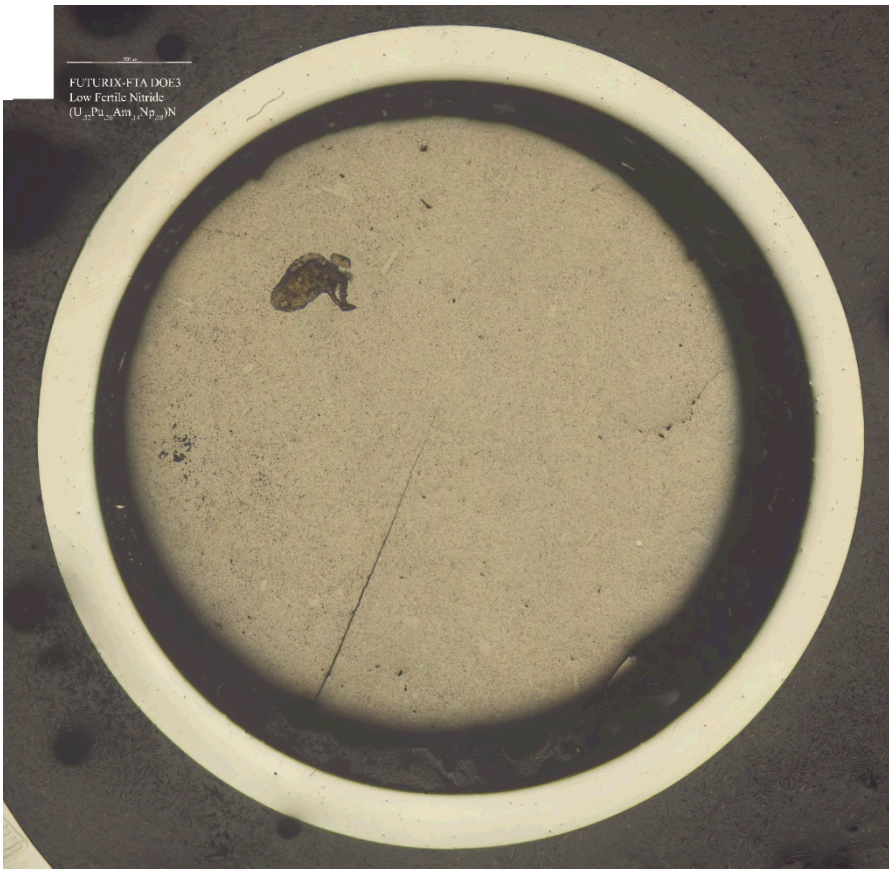

Figure 29. Montage of images collected from cross section of DOE3

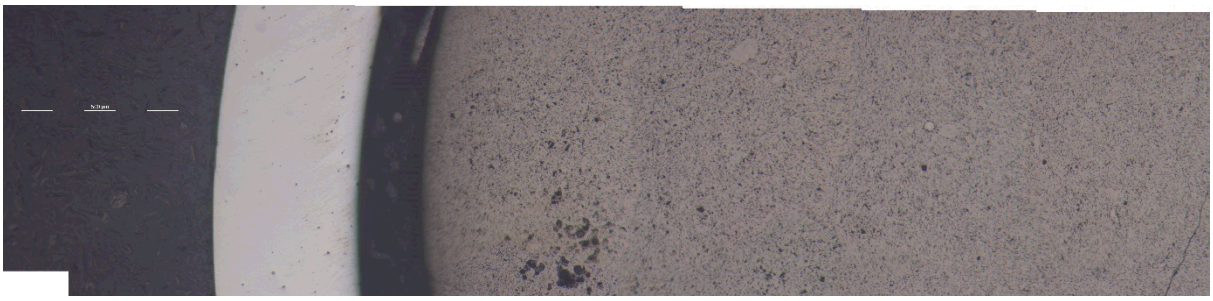

Figure 30. Higher magnification detail of radial microstructure revealed in DOE3

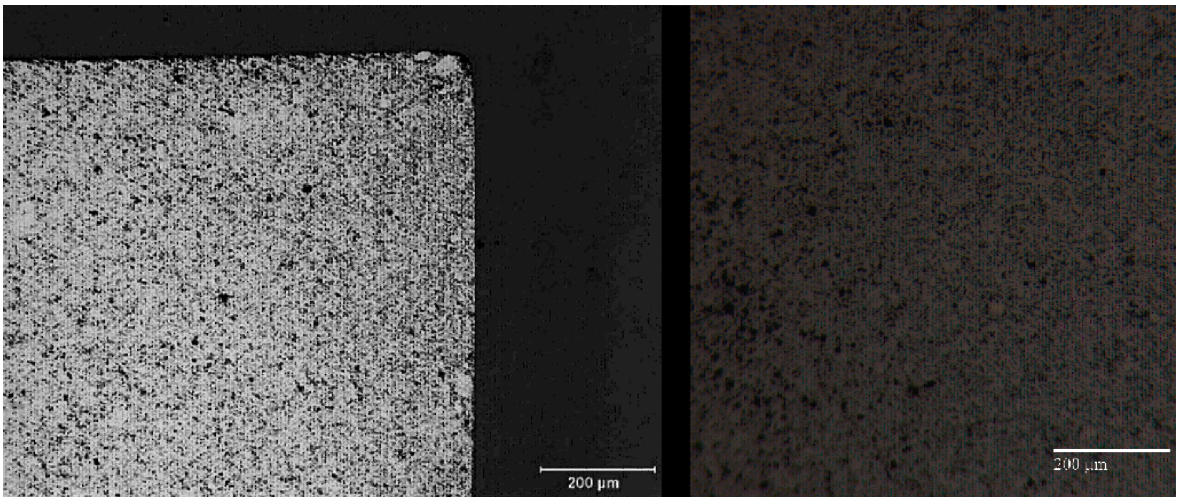

Figure 31. DOE 3 As-fabricated (left) microstructure compared to irradiated microstructure (right)

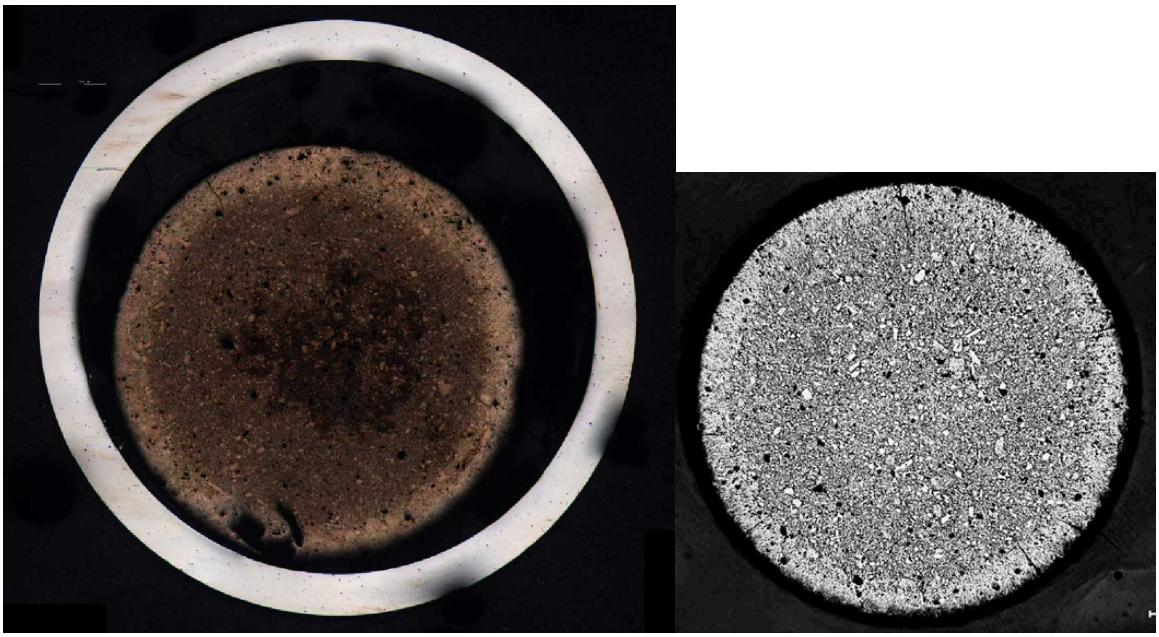
Figure 32. Montage of images collected from cross section of DOE4 (left) compared to the as-fabricated pellet microstructure (right)

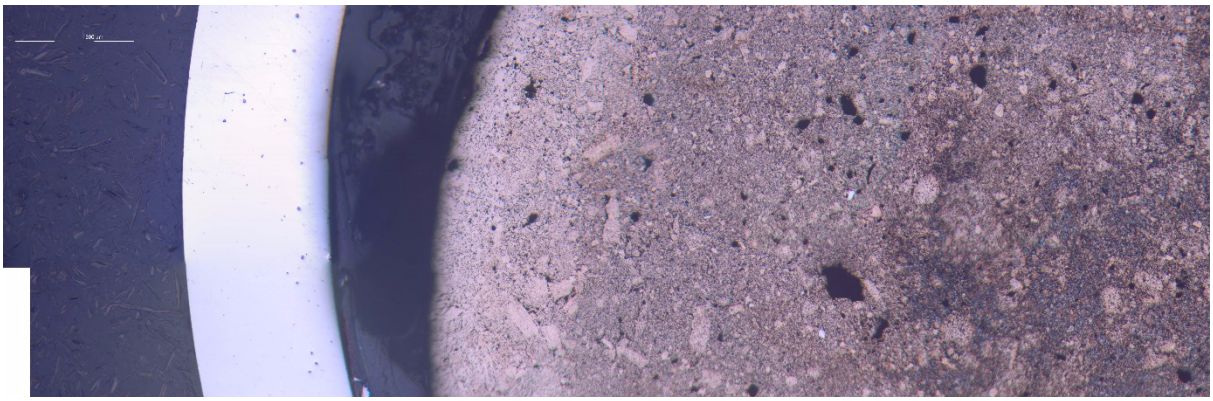

Figure 33. Higher magnification detail of radial microstructure revealed in DOE4

4.3 Analytical Chemistry

During rodlet sectioning to create the microscopy samples, additional samples were taken from near the fuel stack center and sent to the INL Analytical Laboratory (AL) for a variety of chemical and radiological analyses. The primary goal of the analysis is to ascertain the burnup of the sampled material. Gamma spectrometry analysis is also performed. Axial variations in burnup along a rodlet, if any exist, can typically be scaled by comparing quantitative gamma spectrometry results from the AL to semi-quantitative results from PGS. Mass spectrometry analysis can also provide information on the destruction of actinides and minor actinides. Minor actinide destruction is an essential feature of transmutation fuel. An important result from the FUTURIX-FTA experiment is to compare the actinide mix at the end of irradiation to the actinide mix at the end of AFC-1 experiments. Determining if the change in final minor actinide content impacts fuel performance will be important in interpreting future transmutation fuel tests in ATR.

Burnup is calculated from the results of mass spectrometry examinations of dissolved fuel samples. Samples are placed in a heated acid solution until both the fuel alloy or compound and the cladding have dissolved. Care is taken to ensure complete dissolution of all constituents which can take up to 24 hours to complete. Metallic fuel samples were dissolved in 9M HCl. The nitride samples were also dissolved in 9M HCl. During transfer from HFEF to AL the nitride pellet from the DOE4 sample separated from the cladding. This is beneficial as it allows for a good check of the cladding analysis technique.

After initial dissolution, original solutions are saved for archive or if a reanalysis is necessary. Aliquots of the original dissolution are diluted and sent through different inductively coupled plasma mass spectrometry devices (ICP-MS). Samples are sent through an ICP-AES (atomic emission spectrometry) to determine the cladding and sodium weight of the sample. The derived cladding weight is then subtracted from the balance measured as-received sample mass. Samples are removed from the hot-cell and sent through an ICP-MS to determine the isotopic composition of the major constituents and fission products. In many cases there are isobaric (same atomic number) interferences that prevent exact identification of isotopic species. In the fission product data, isobaric interferences were not considered significant to the conclusions of this study, so no additional separations were performed to clear these interferences. The primary isobaric interferences in the actinides are from Pu. To remove the Pu from the solutions, they are passed through an Eichrom TEVA Resin. Pu is retained in the resin and all other actinides pass through. The Pu solution and the mixed actinide (Th, U, Np, Am, Cm) are analyzed by the ICP-MS. Ideally the Am and Cm interferences would be further resolved using an additional separation or alpha spectrometry, but these techniques were not available at the time of the analysis. The ICP-MS results were able to produce isotope specific results for U-234, U-235, U-236, U-238, Pu-238, Pu-239, Pu-240, Pu-241, Pu-242, Np-237, Am-241, and Cm-244. The combined mass of Am-242 and Cm-242 was evaluated as well as the combined mass of Am-243 and Cm-243. Higher mass minor actinides were not measured in detectable quantities. The final results from AL are archived as AL reports (log number 99526, 99527, 99528, and 99529). These reports can also be found in Appendix C.

The determination of burnup was performed using the measured mass of a specific fission product in the fuel, the cumulative fission yield of that specific fission product, and the total mass of actinides present in the sample. This method is sometimes referred to as the "Fission Product Monitor - Residual Heavy Atom" technique [24, 25]. Ideally, the fission products used in the calculations should have a small neutron absorption cross section, a high cumulative fission yield, and a similar fission yield for that nuclear isobar between U and Pu fission. Chemically the fission product must also readily dissolve during the dissolution process. This technique uses the following formula to calculate burnup (BU) based on a specific fission product detected in the ICP-MS spectrum. Burnup is calculated in % fission per initial heavy metal atoms (FIMA) which is comparable to heavy metal depletion and atom % burnup units used in other sources.

Table 5. Burnup values for FUTURIX-FTA

Name	Composition*	Simulation[15,16] (%FIMA)	Measured Burnup (%FIMA)	Measured Fission Density (fissions/ cm^3)
DOE1	U-28.3Pu-3.8Am-2.1Np-31.7Zr	9.08%	9.53%	2.08E+21
DOE2	Pu-10.5Am-0.3Np-41.6Zr	15.50%	12.67%	2.01E+21
DOE3	$(U_{0.51}Pu_{0.27}Am_{0.14}Np_{0.08})N$	1.57%	1.43%	4.50E+20

$$BU = \frac{\left(N_{fp} / y_{fp}\right)}{\left(\left(N_{fp} / y_{fp}\right) + N_{Act}\right)} \times 100 \quad (1)$$

Where N_{fp} is number of atoms of a specific fission product *fp* measured in the sample, y_{fp} is the cumulative fission yield of fission product *fp*, and N_{Act} is the number of atoms of actinides in the sample. All fission yields were taken from ENDF/B-VII.1 [26]. A benefit of this burnup technique is that it requires no *a priori* knowledge of the sample. All the factors in Equation 1 can be directly measured from mass spectrometry results and no assumptions about the pre-irradiation state of the fuel or the size of the sampled material need to be made. The described technique is largely similar to the more standardized Nd-148 burnup technique (ASTM E321). However ASTM E321 requires a difficult Nd separation to remove Sm-148 and a correction to account for neutron absorption in Nd-148 that is only valid for thermal spectrum systems. Historically the "Fission Product Monitor - Residual Heavy Atom" technique has performed quite well in the evaluation of EBR-II fuel. For this burnup analysis the fast fission yields were used in the calculation of burnup. The feedstock uranium in the low-fertile samples was depleted U, so U-235 fission was not considered. The burnup would be biased if only the Pu-239 cumulative fast fission yields were used in Equation (1) for burnup determination. In order to estimate the fraction of fission that occurred in a particular isotope, the effective fission yield for several isotopes was assumed to be a weighted average between the yields for Pu-239, U-238, Am-241, and Pu-240. The weighted average for each sample was determined by finding the weights that minimized the burnup spread among the six key fission product burnup indicators for this technique (La-139, Ce-140, Ce-142, Pr-141, Nd-145, and Nd-146). Using this minimization technique it was possible to assume that for DOE1 81% of the fission came from Pu-239 and 19% came from U-238 fast fissions, for DOE3 85% of fission came from Pu-239 and 15% came from U-238, and for DOE2 and DOE4 all fission came from Pu-239. These assumptions are likely adequate for the uncertainty of the mass spectrometry data which is ±5% (2 sigma).

There are six isotopes that work reliably for the ICP-MS technique in the FUTURIX-FTA fuel: La-139, Ce-140, Ce-142, Pr-141, Nd-145, and Nd-146. These isotopes occur on the higher atomic number peak of the bimodal fission product distribution. They are all lanthanides that will readily dissolve in the selected acid. The differences between fission yields are fairly small for these isotopes as well. All these isotopes are nonradioactive and have relatively small neutron absorption cross section with the exception of Nd-145. Because of its cross section, the number of Nd-145 and Nd-146 atoms in the samples and their respective yields are summed in the calculation of burnup. In this calculation, the burnup measurement for each sample of particles was found by taking the average of the individual isotope results from Equation (1) for La-139, Ce-140, Ce-142, Pr-141, and the Nd-145 + Nd-146 combined result. The uncertainty of all mass spectrometry values is ±5% (2 sigma), and the derived burnup values are also considered no better than 5% relative uncertainty. The measured burnup values, the measured fission

DOE4

*numbers preceding elements denote weight percent, subscript numbers represent mole percent. This is the as-fabricated composition not the nominal composition

5. Summary

Baseline PIE is now complete for the FUTURIX-FTA Pins. This examination includes visual examination, neutron radiography, gamma spectrometry scanning, dimensional inspection, fission gas release evaluation, optical microscopy, and chemical analysis. All indications are the fuel performed well during the irradiation. While these exams have provided an engineering or macroscopic scale test of this fuel, samples are now ready and available for a more detailed phenomenological study of the observed performance. There are also likely phenomena that were not possible to observe utilizing baseline PIE techniques. Additional PIE such as electron microscopy will need to be pursued to understand Am behavior in the fuel and also to determine if any initial rare earth attack has begun on the cladding. The completion of the baseline PIE will now initiate efforts to comprehensively compare this irradiation to the AFC-1 irradiations and other similar minor actinide irradiations.

The raw data from the FUTURIX-FTA exams is archived in a shared directory on an Idaho National Laboratory server. Access to this directory from the INL internal network can be arranged by contacting the authors of this report. (\\Fn2\projects\AFC ATF PIE Dat\FUTURIS-FTA)

Acknowledgements

This work was supported by the U.S. Department of Energy, Office of Nuclear Energy. The authors would also like to acknowledge the engineers and operators of HFEF for performing the hot-cell activities that support this work. The authors would also like to acknowledge the staff of the AL who performed the chemical analysis. Specifically Jeffrey Giglio who performed the mass spectrometry and Daniel Cummings who summarized the mass spectrometry results into their final values.

6. References

1. B. Hilton, D. Porter, S. Hayes, "AFC-1 Transmutation Fuels Post-Irradiation Hot Cell Examination 4 to 8 at.% Final Report; Irradiation Experiments AFC-1B, AFC-1F and AFC-1Æ," INL/EXT-05-00785, Rev. 1, September 2006.
2. H.J.M Chichester, D.L. Porter, B.A. Hilton, "Postirradiation Examination of AFC-1D, 1G, 1H, and 2A Experiments," INL/LTD-11-23242, Rev. 0, September 2011.
3. Report to Congress on the Advanced Fuel Cycle Initiative: The Future Path for Advanced Spent Fuel Treatment and Transmutation Research, U.S. Department of Energy Office of Nuclear Science and Technology, January 2003
4. G.L. Hofman, L.C. Walters, T.H. Bauer, Metallic fast reactor fuels, Progress in Nuclear Energy, Volume 31, Issues 1–2, 1997, Pages 83-110, ISSN 0149-1970, http://dx.doi.org/10.1016/0149-1970(96)00005-4.
5. G.L. Hofman, S.L. Hayes, M.C. Petri, Temperature gradient driven constituent redistribution in U‧ Zr alloys, Journal of Nuclear Materials, Volume 227, Issue 3, January 1996, Pages 277-286, ISSN 0022-3115, http://dx.doi.org/10.1016/0022-3115(95)00129-8.
6. Douglas C. Crawford, Douglas L. Porter, Steven L. Hayes, Fuels for sodium-cooled fast reactors: US perspective, Journal of Nuclear Materials, Volume 371, Issues 1–3, 15 September 2007, Pages 202-231, ISSN 0022-3115, http://dx.doi.org/10.1016/j.jnucmat.2007.05.010.
7. W.J. Carmack, D.L. Porter, Y.I. Chang, S.L. Hayes, M.K. Meyer, D.E. Burkes, C.B. Lee, T. Mizuno, F. Delage, J. Somers, Metallic fuels for advanced reactors, Journal of Nuclear Materials, Volume 392, Issue 2, 15 July 2009, Pages 139-150, ISSN 0022-3115, http://dx.doi.org/10.1016/j.jnucmat.2009.03.007.
8. T. Ogata, 3.01 - Metal Fuel, In Comprehensive Nuclear Materials, edited by Rudy J.M. Konings,, Elsevier, Oxford, 2012, Pages 1-40, ISBN 9780080560335, http://dx.doi.org/10.1016/B978-0-08-056033-5.00049-5
9. Y. Arai, 3.02 - Nitride Fuel, In Comprehensive Nuclear Materials, edited by Rudy J.M. Konings,, Elsevier, Oxford, 2012, Pages 41-54, ISBN 9780080560335, http://dx.doi.org/10.1016/B978-0-08-056033-5.00050-1
10. H.J.M. Chichester, *et al.*, "Overview of the FUTURIX-FTA Irradiation Experiment in the Phénix Reactor," Proceedings of Global 2015, Paper 5268, 2015, Paris, France
11. Jin Sik Cheon, Chan Bock Lee, Byoung Oon Lee, J.P. Raison, T. Mizuno, F. Delage, J. Carmack, Sodium fast reactor evaluation: Core materials, Journal of Nuclear Materials, Volume 392, Issue 2, 15 July 2009, Pages 324-330, ISSN 0022-3115, http://dx.doi.org/10.1016/j.jnucmat.2009.03.021
12. Gavoille, P., et al. "Mechanical properties of cladding and wrapper materials for the ASTRID Fast-Reactor Project." *Proc. of the IAEA International Conference on Fast Reactors and related Fuel Cycles: Safe Technologies and Sustainable Scenarios*. 2013.
13. J. R. Kennedy, "FUTURIX-FTA Metal Alloy Fuel Fabrication and Characterization Report," INL Report INL/EXT-07-12234 (2007).
14. S. Voit, K. McClellan, R. Margevicius, C. Stanek, and H. Hawkins, "The Design and Production of Actinide Nitride Fuels at the Los Alamos National Laboratory for the Advanced Fuel Cycle Initiative Program," LANL Report LA-UR-06-4930 (2006).
15. I. Munoz, C. Repetto, B. Valentin, "Irradiation Report of the FUTURIX-FTA Metal Capsule," Note Technique, CEA/DEN/CAD/DEC/SESC/LC2I NT 12-020 – Indice 1, Commissariat à l'Energie Atomique et aux Energies Alternatives (CEA) Report, CEA Cadarache, June 2014
16. I. Munoz, C. Repetto, B. Valentin, "Irradiation Report of the FUTURIC-FTA Nitride Capsule," Note Technique, CEA/DEN/CAD/DEC/SESC/LC2I NT 09-004 – Indice 2, Commissariat à l'Energie Atomique et aux Energies Alternatives (CEA) Report, CEA Cadarache, June 2014
17. J.M. Harp, P.A. Demkowicz, "Investigation of the Feasibility of Utilizing Gamma Emission Computed Tomography in Evaluating Fission Product Migration in Irradiated TRISO Fuel Experiments," Proceedings of HTR 2014, Weihai, China, October 27-31 2014
18. John D. Hunn, Charles A. Baldwin, Tyler J. Gerczak, Fred C. Montgomery, Robert N. Morris, Chinthaka M. Silva, Paul A. Demkowicz, Jason M. Harp, Scott A. Ploger, Detection and analysis of particles with failed SiC in AGR-1 fuel compacts, Nuclear Engineering and Design, Volume 306, September 2016, Pages 36-46, http://dx.doi.org/10.1016/j.nucengdes.2015.12.011
19. Jason M. Harp, Heather J.M. Chichester, "Highlights from the Postirradiation Examination of AFC-3A and AFC-3B." *Transactions of the American Nuclear Society,* vol. 114, 2016
20. Personal Communication, Douglas C. Porter, X419 PIE archive data
21. R.S. Fielding, "FUTURIX-FTA Short Fuel Pin Welding Procedure," Idaho National Laboratory Record,

W7520-0709-ES-00, Rev. 0, July 2006
22. R.G. Pahl, D.L. Porter, D.C. Crawford, L.C. Walters, Irradiation behavior of metallic fast reactor fuels, Journal of Nuclear Materials, Volume 188, 1992, Pages 3-9, http://dx.doi.org/10.1016/0022-3115(92)90447-S
23. D.E. Janney, C.A. Papesch, "2015. *FCRD Transmutation Fuels Handbook 2015,"* Idaho National Laboratory Report, INL/EXT-15-36520, Idaho National Laboratory (INL), Idaho Falls, ID (United States).
24. Maeck, W.J., Larsen, R.P., Rein, J.E., "Burnup Determination for Fast Reactor Fuels: A Review and Status of the Nuclear Data and Analytical Chemistry Methodology Requirements," NTIS Report TID 26209, 1973
25. J.M. Harp, P.A. Demkowicz, P.L. Winston, J.W. Sterbentz, "An analysis of nuclear fuel burnup in the AGR-1 TRISO fuel experiment using gamma spectrometry, mass spectrometry, and computational simulation techniques," Nuclear Engineering and Design, 278, 395-405, (2014) http://dx.doi.org/10.1016/j.nucengdes.2014.07.041
26. Chadwick, M. B., et al. "ENDF/B-VII. 1 nuclear data for science and technology: cross sections, covariances, fission product yields and decay data." Nuclear Data Sheets 112.12: 2887-2996. 2011

Position A

Image 1

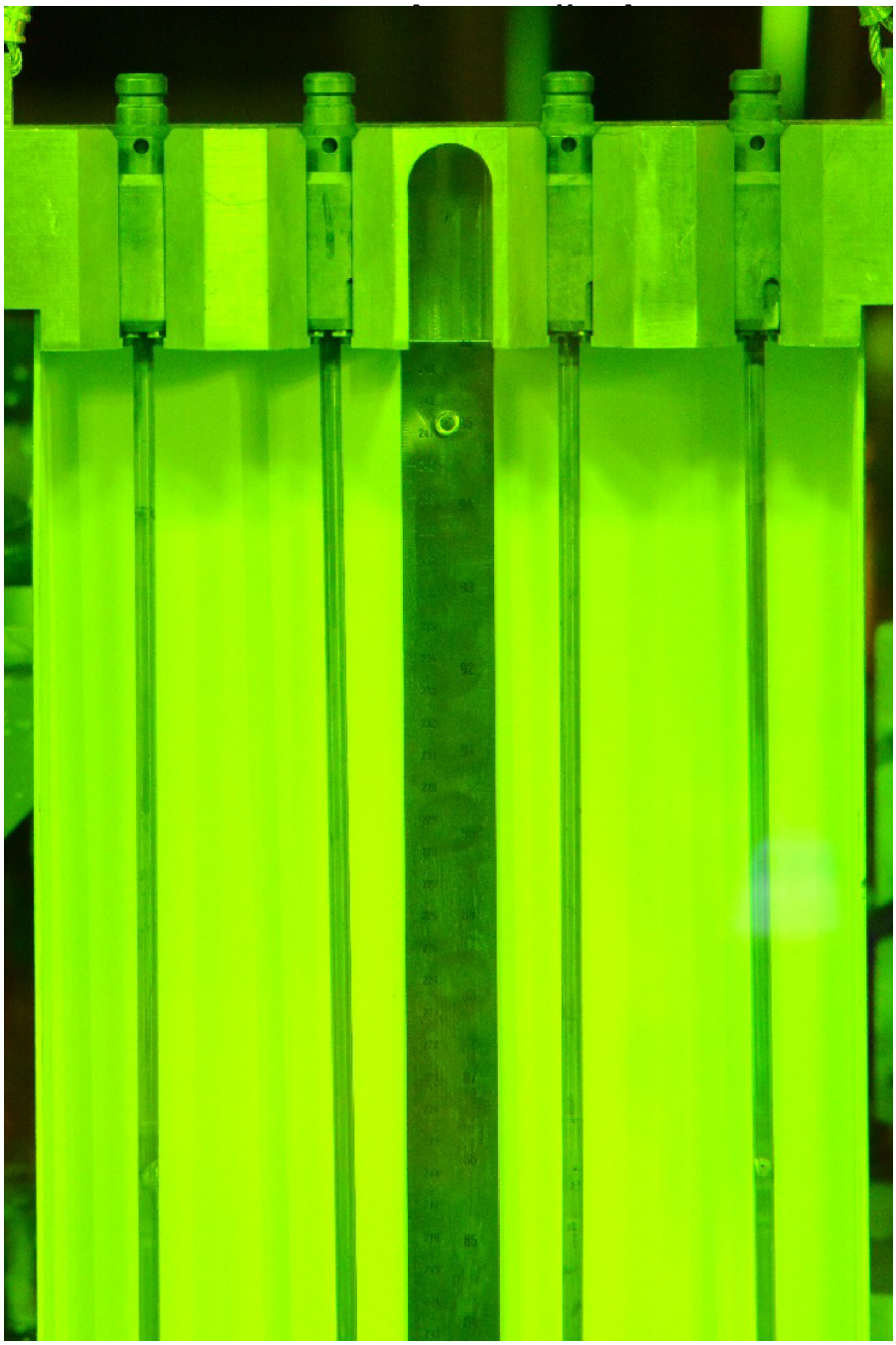

Image 2

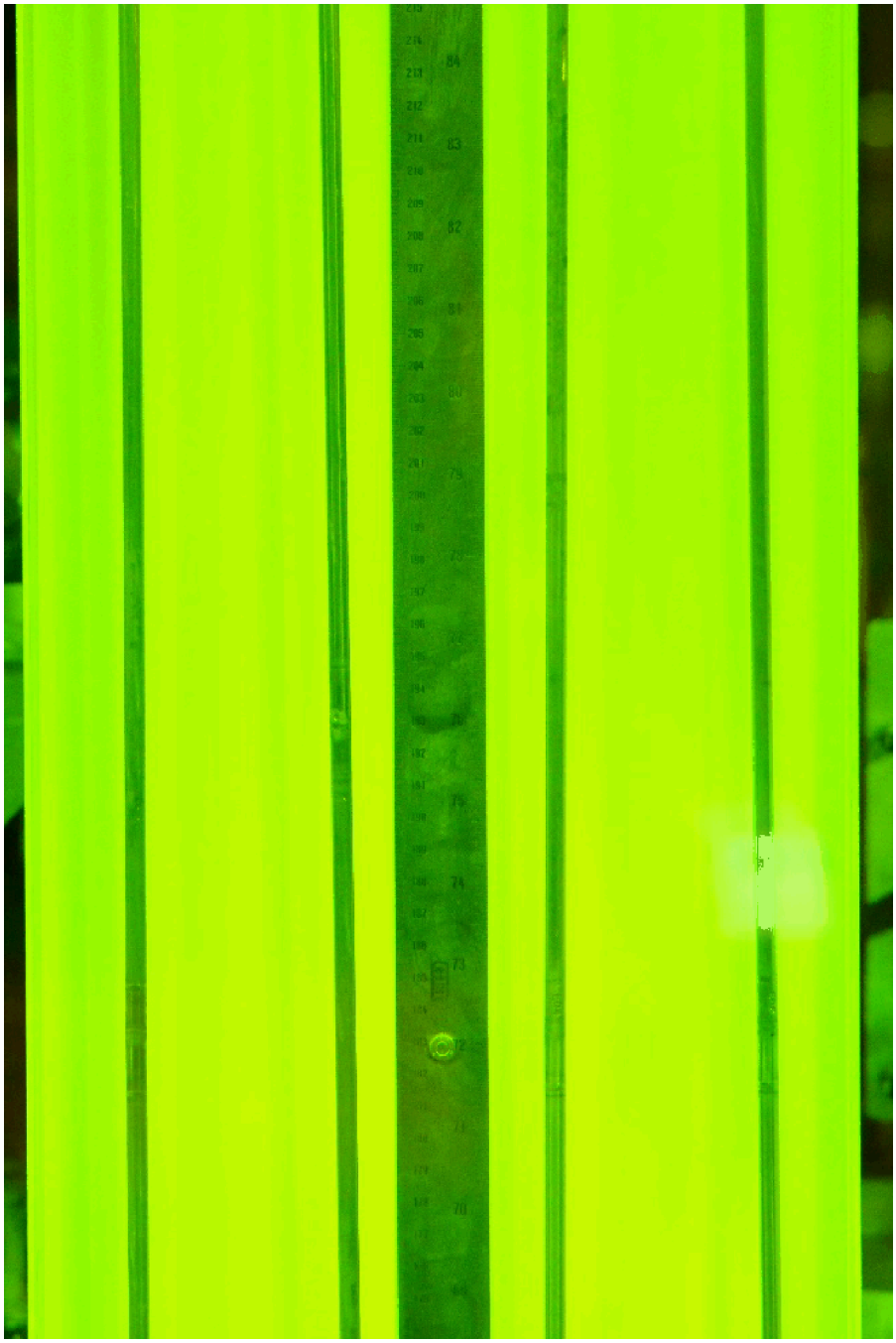

Image 3

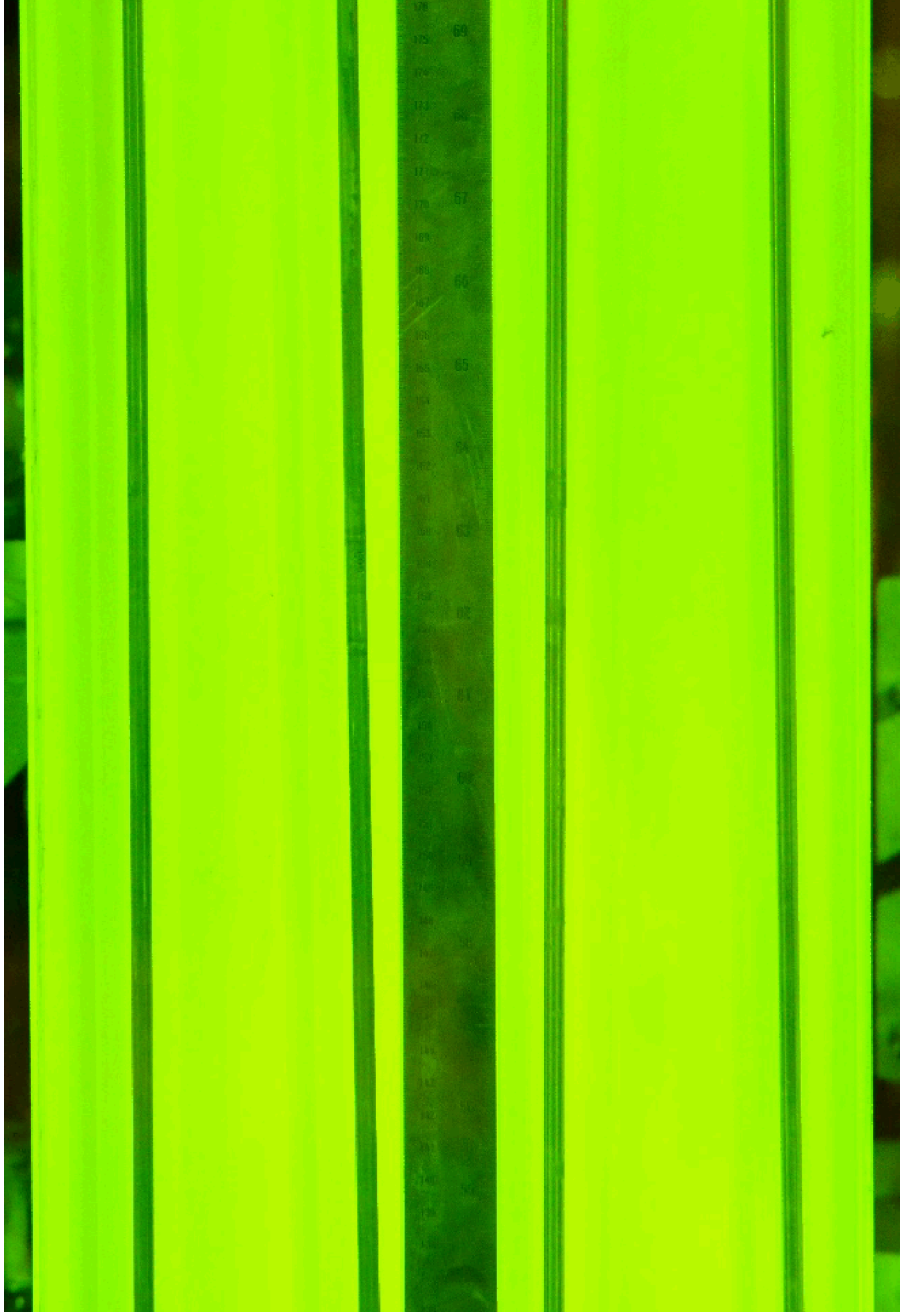

Image 4

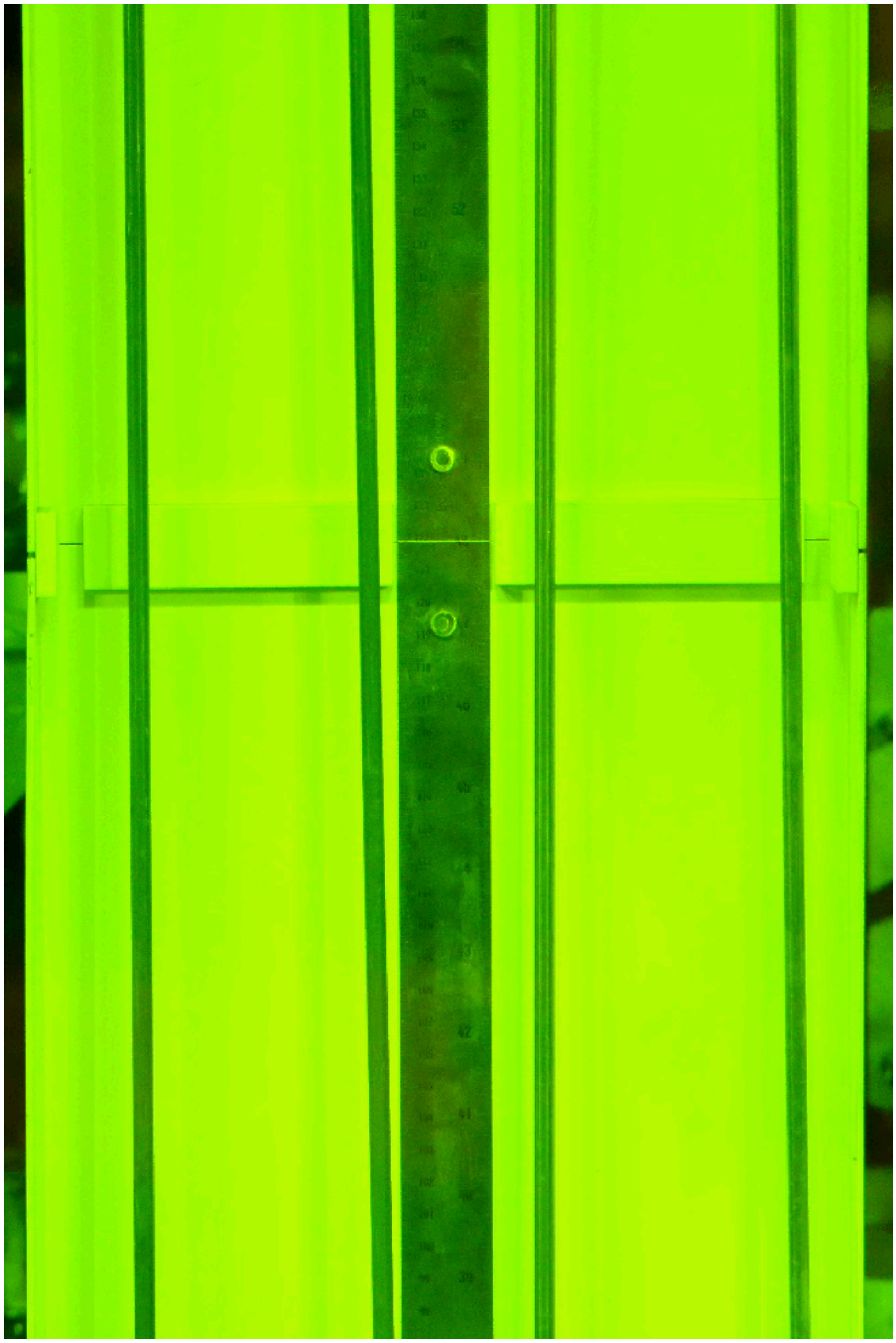

Image 5

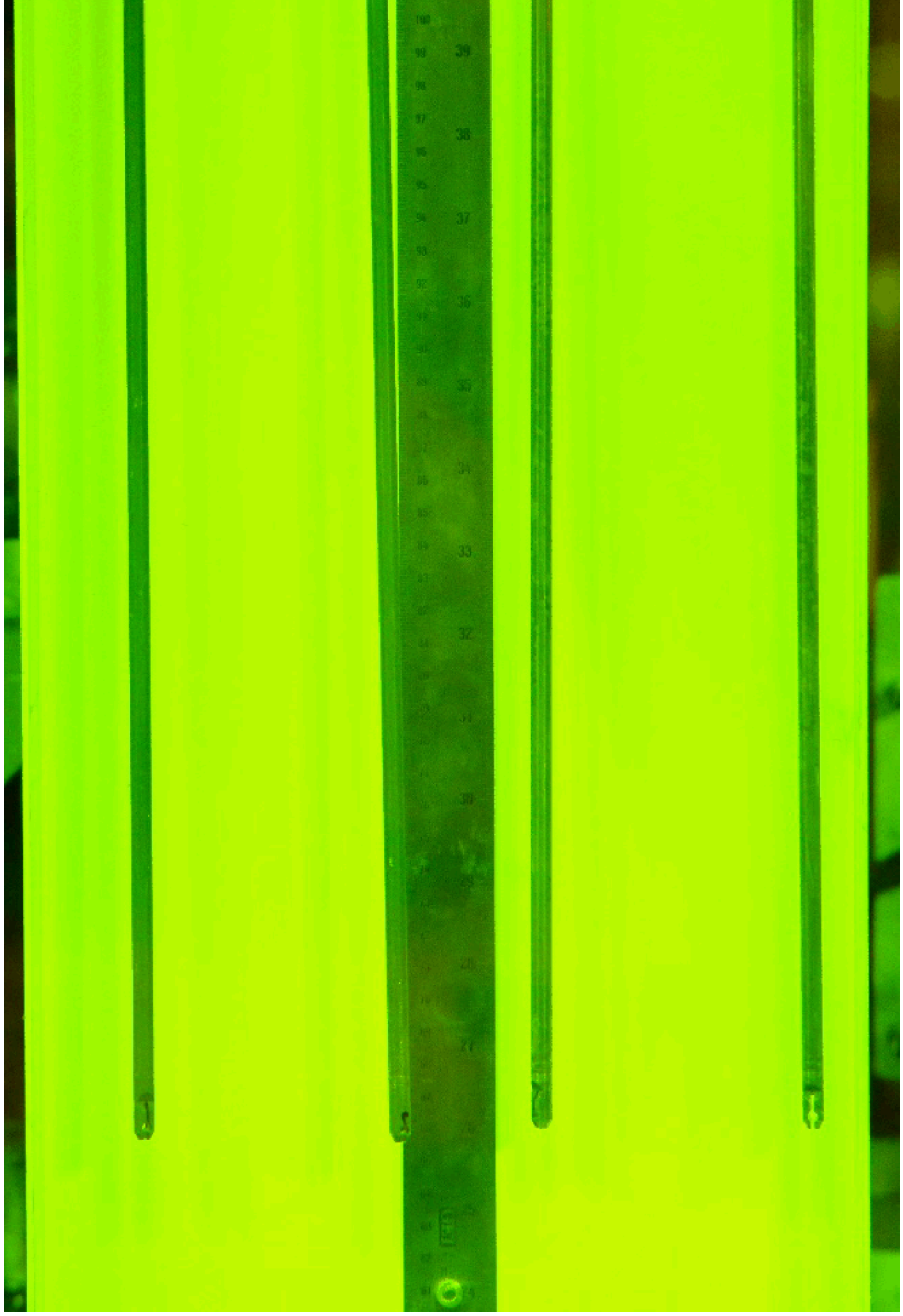

Position B (180° Ro

Image 1

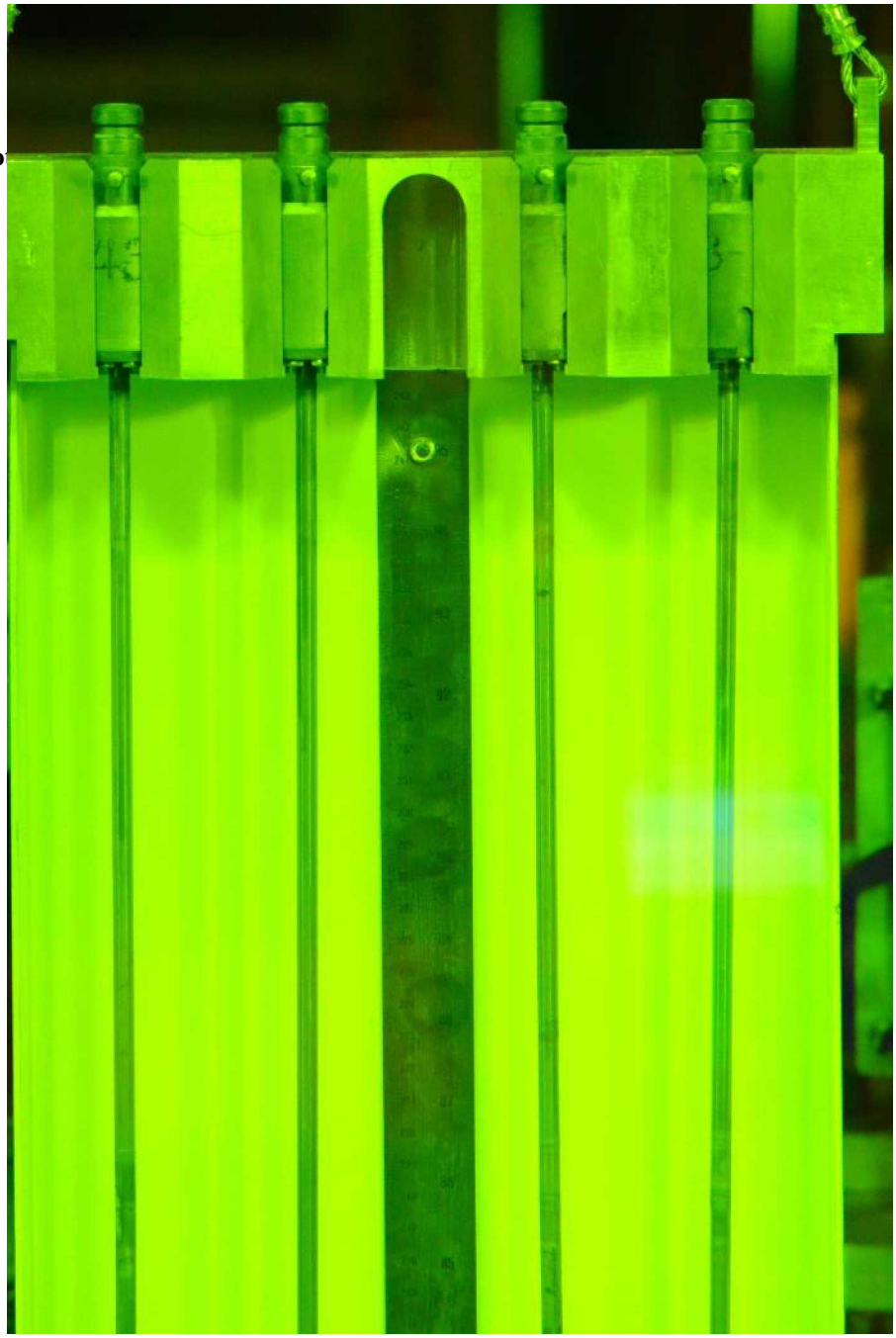

Image 2

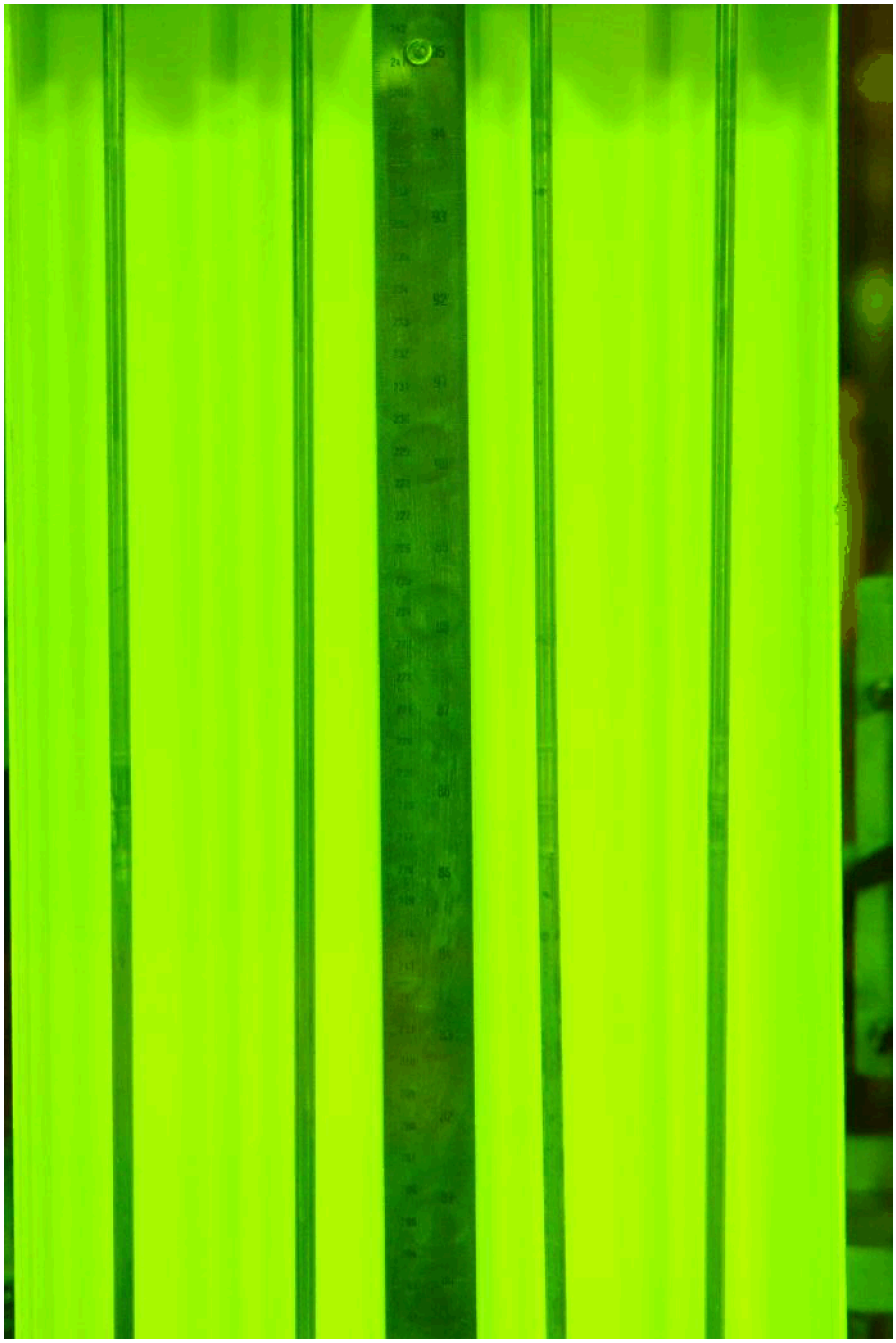

Image 3

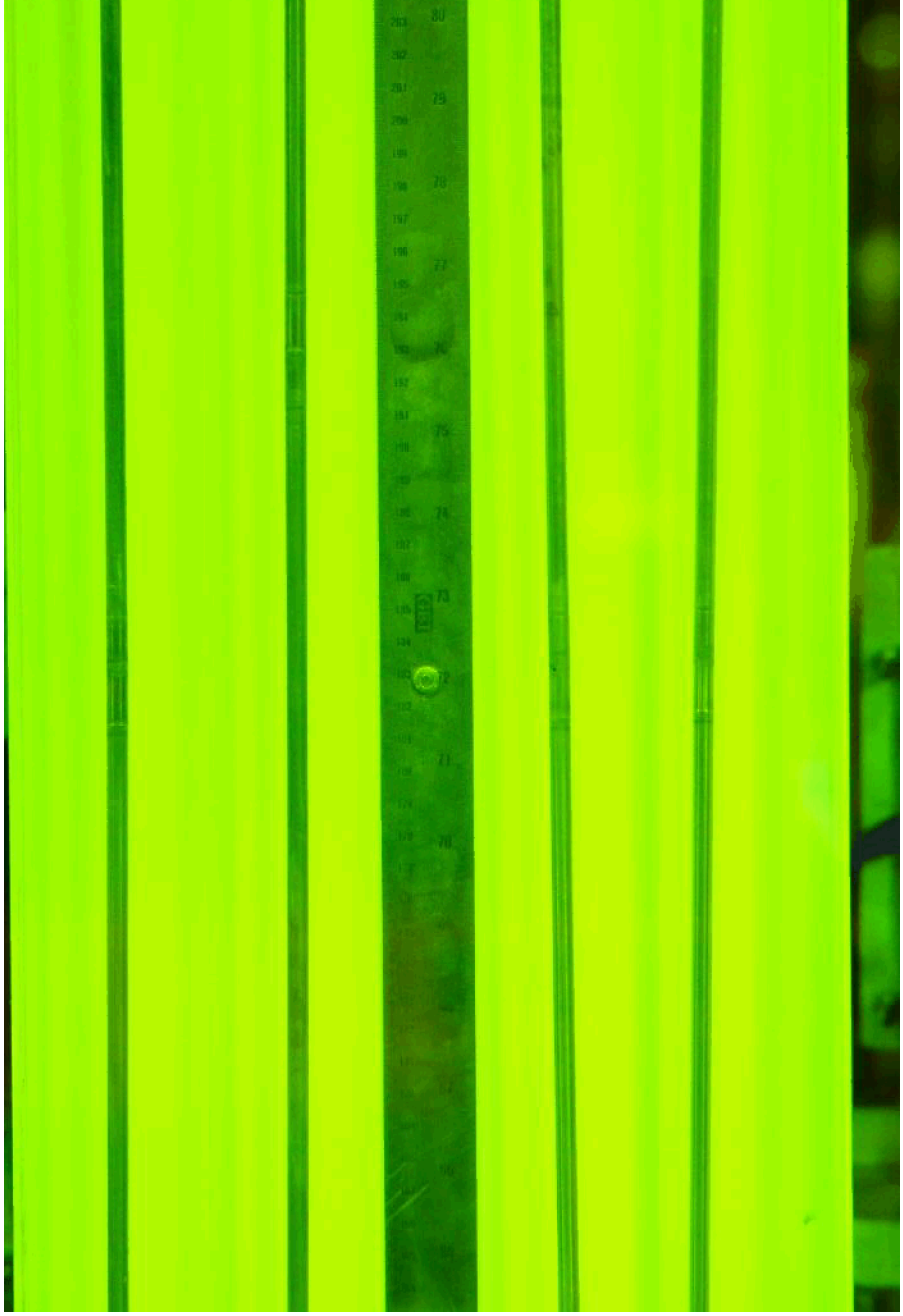

Image 4

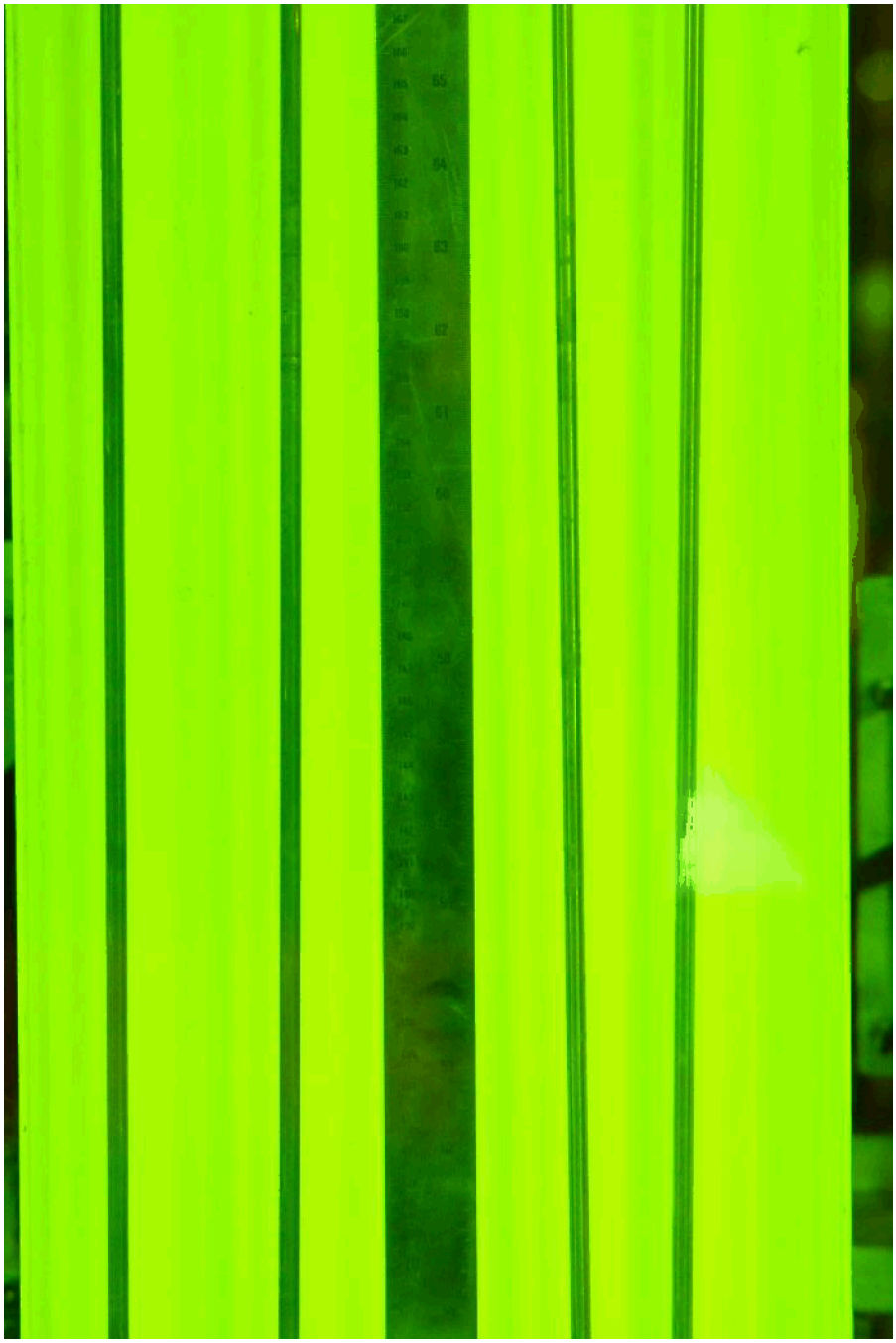

Image 5

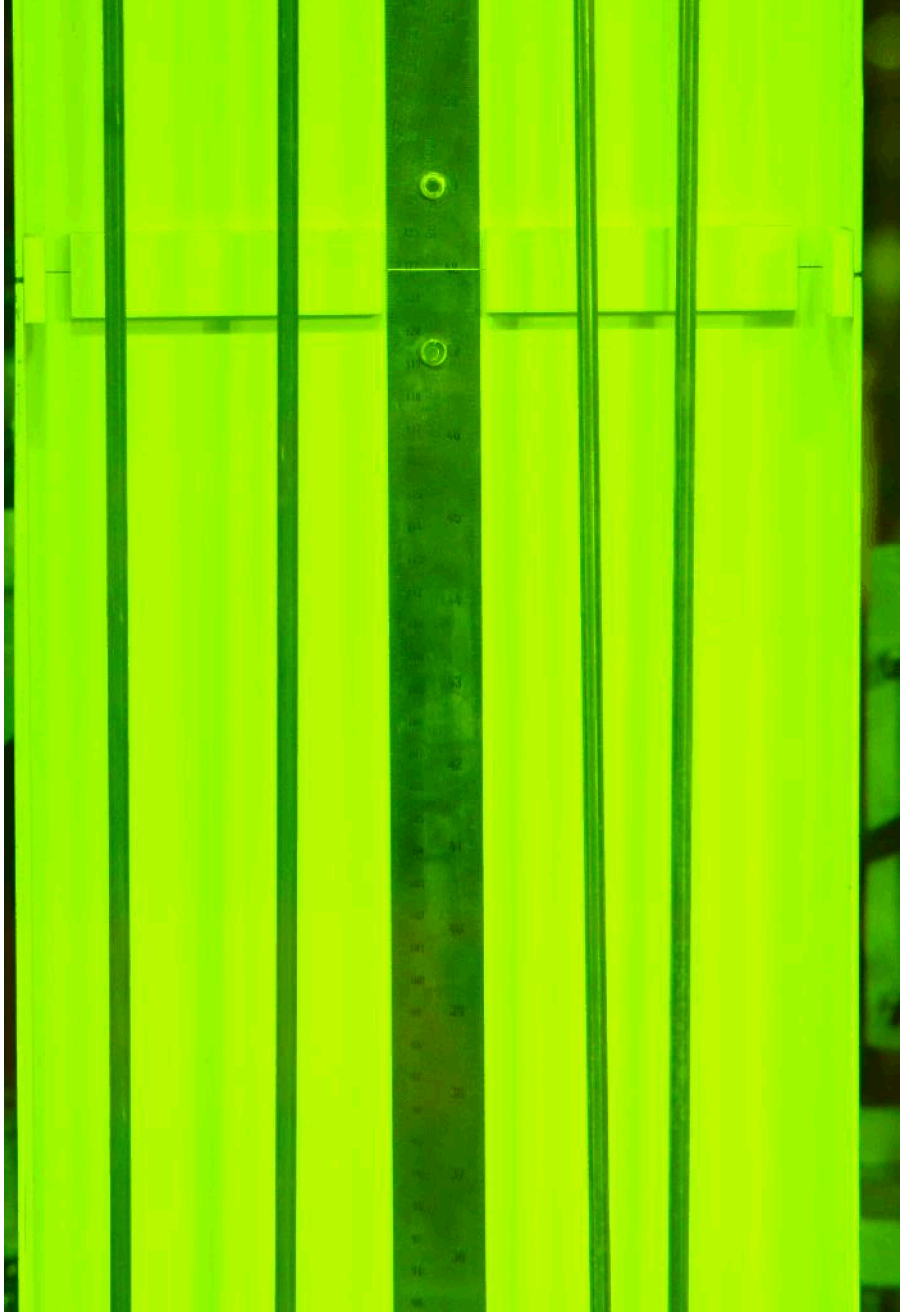

Image 6

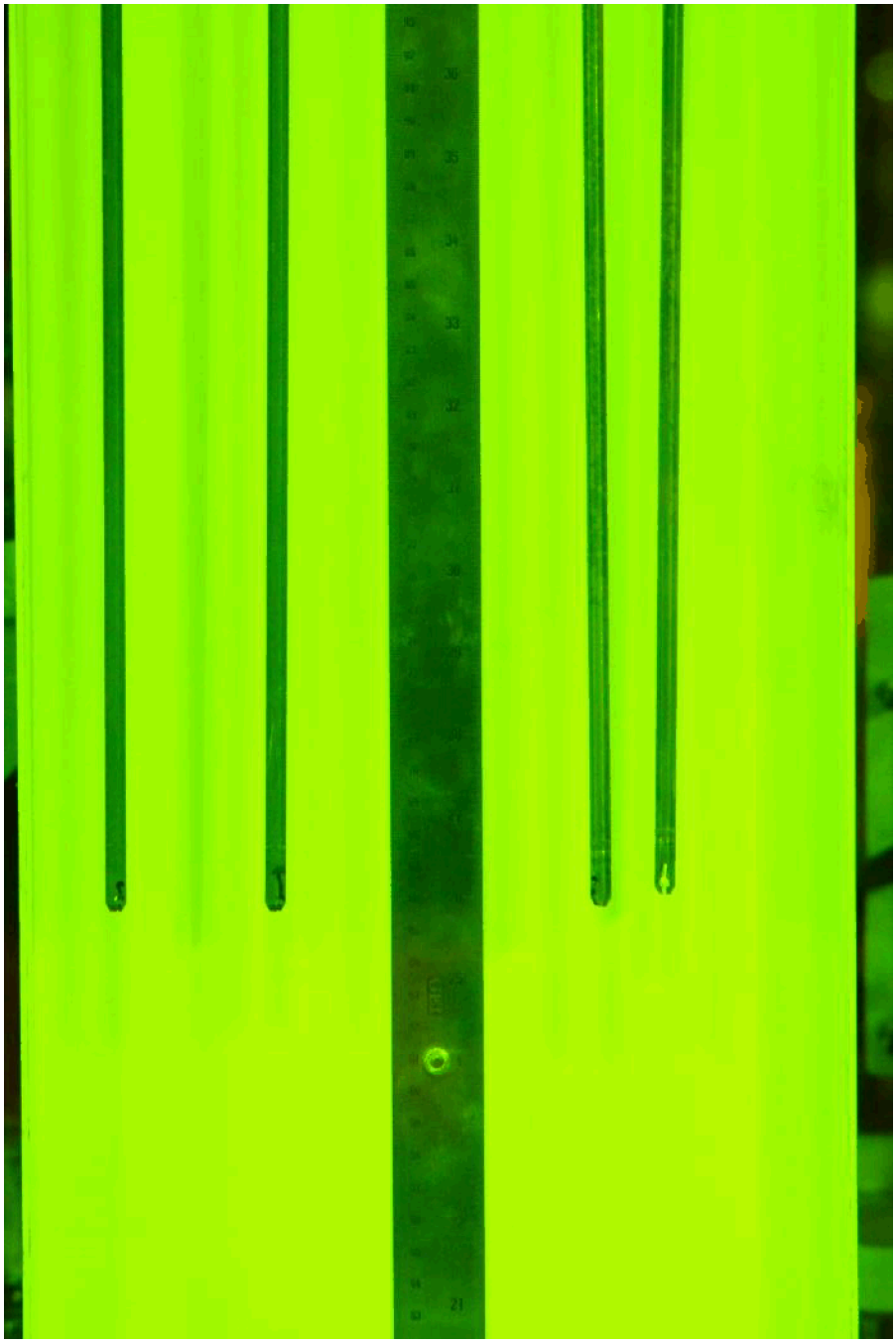

Appendix B

Neutron Radiography of FUTURIX-FTA

Thermal Angle 1

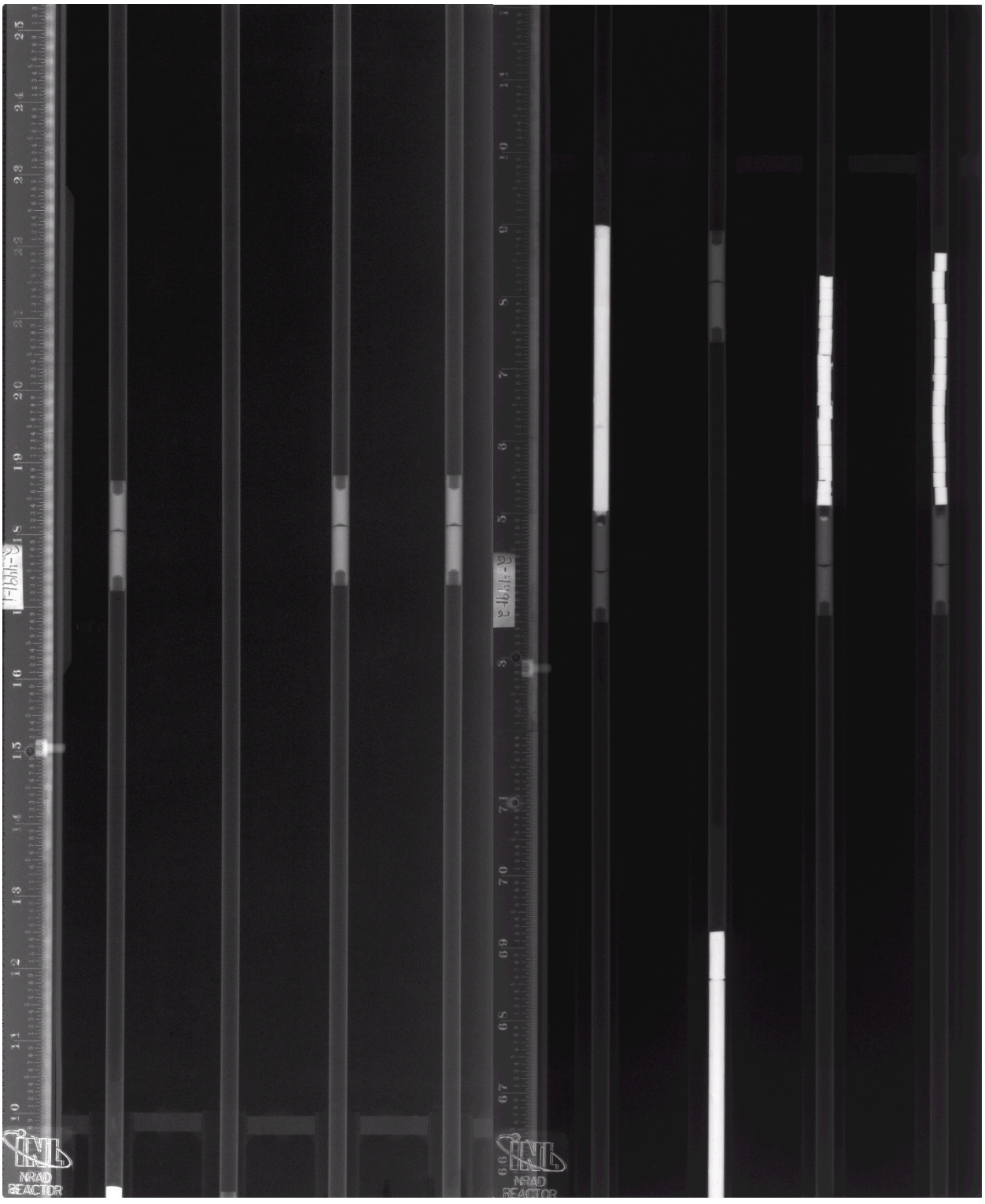


INL
NRAD
REACTOR
INL
NRAD
REACTOR

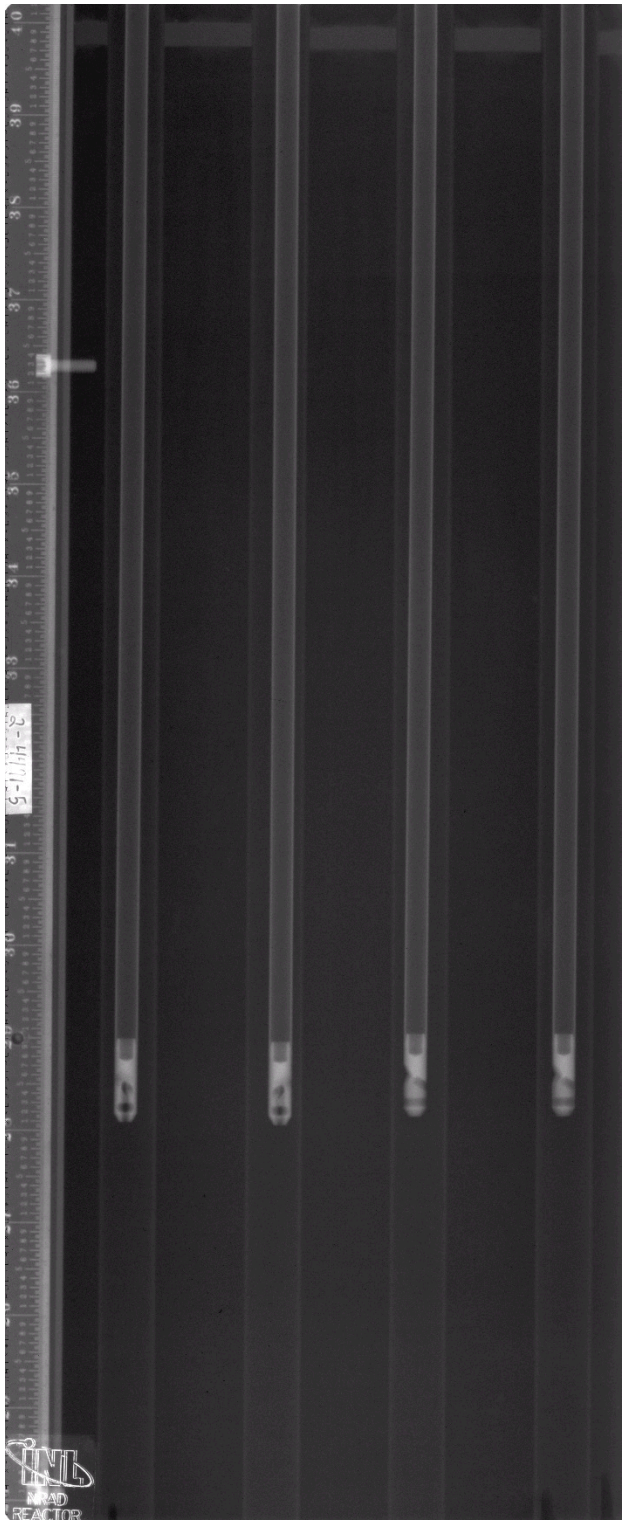
INL
NRAD
REACTOR

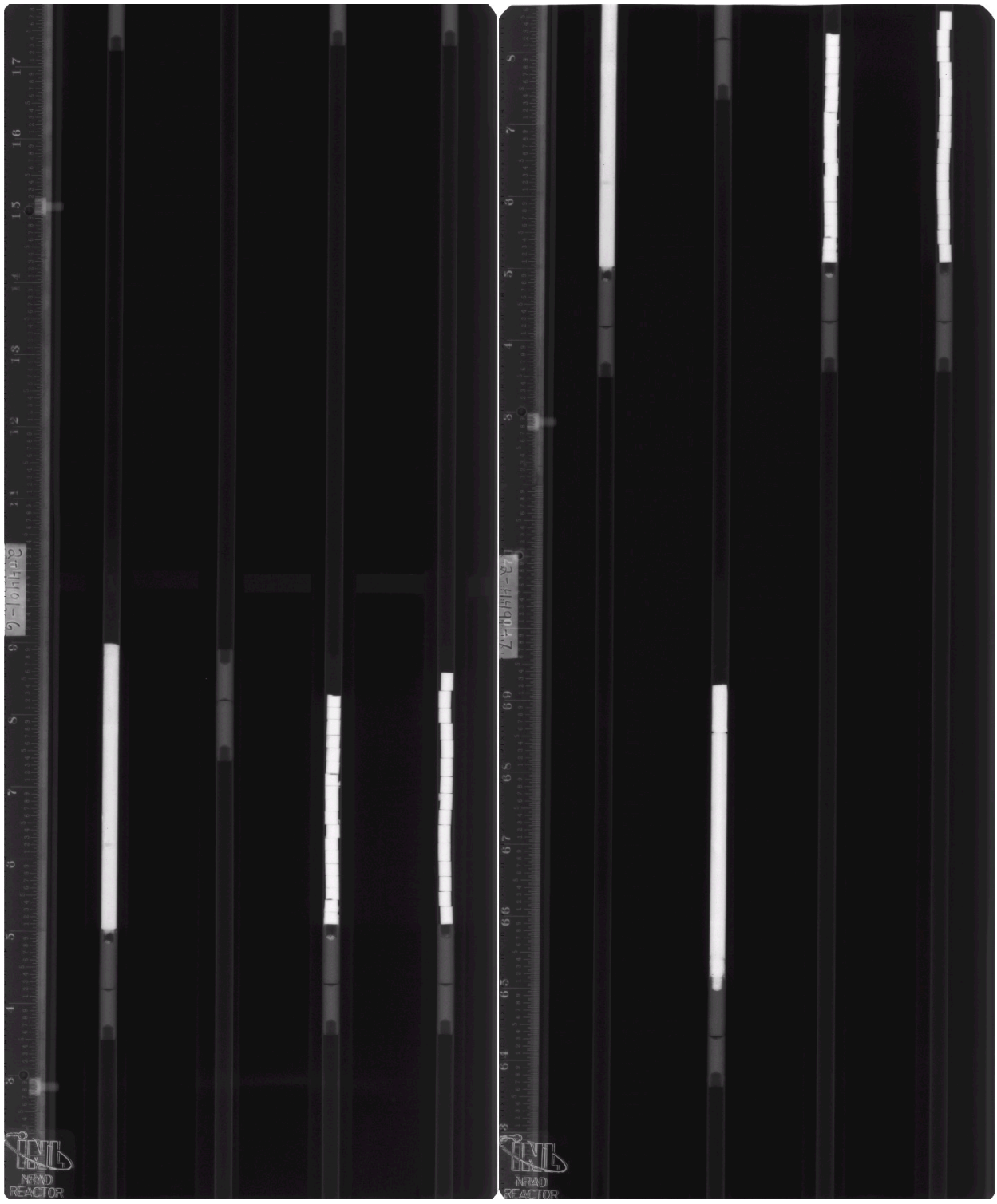
INL
NRAD
REACTOR
INL
NRAD
REACTOR

Thermal Angle 2

Epithermal Angle 1

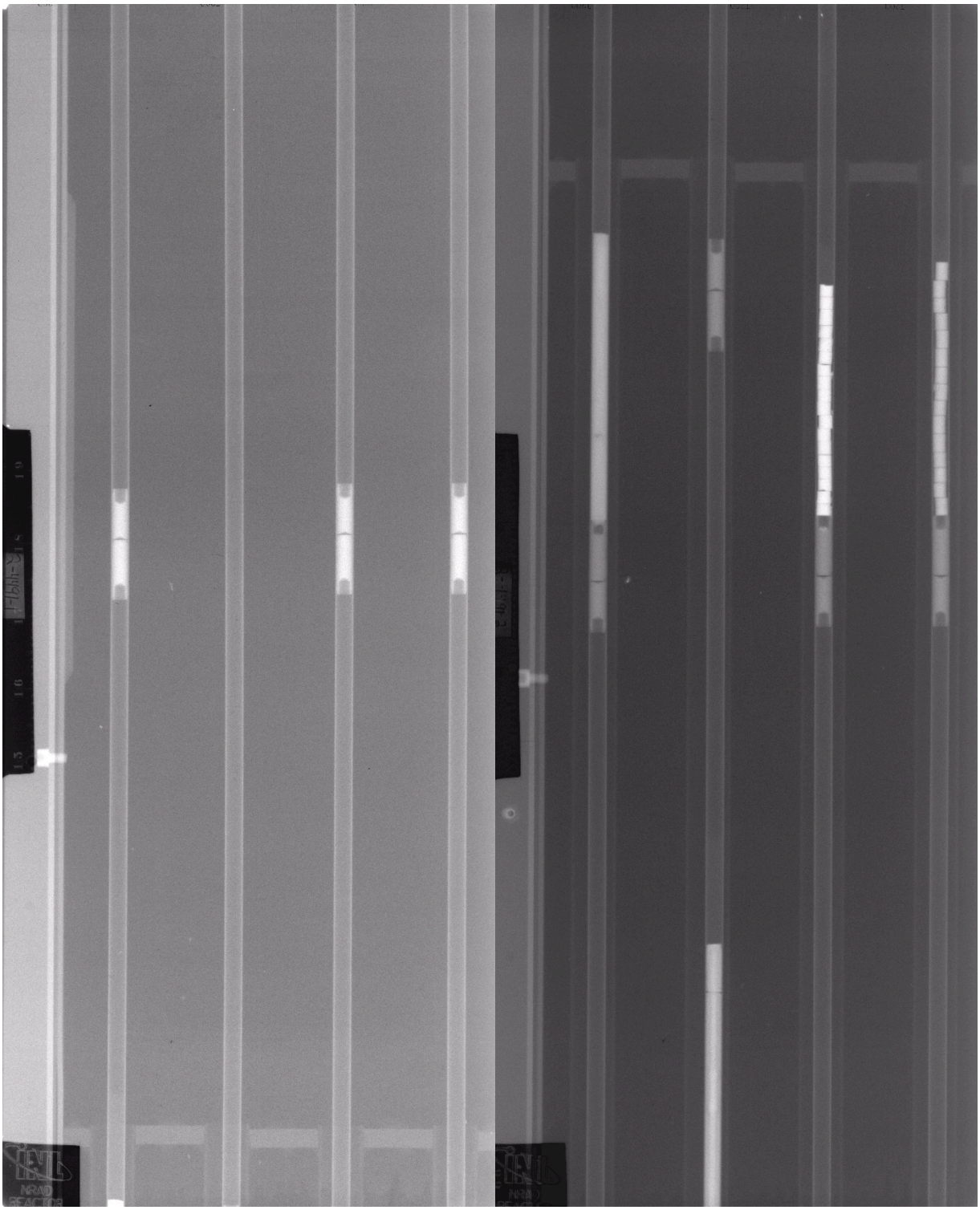

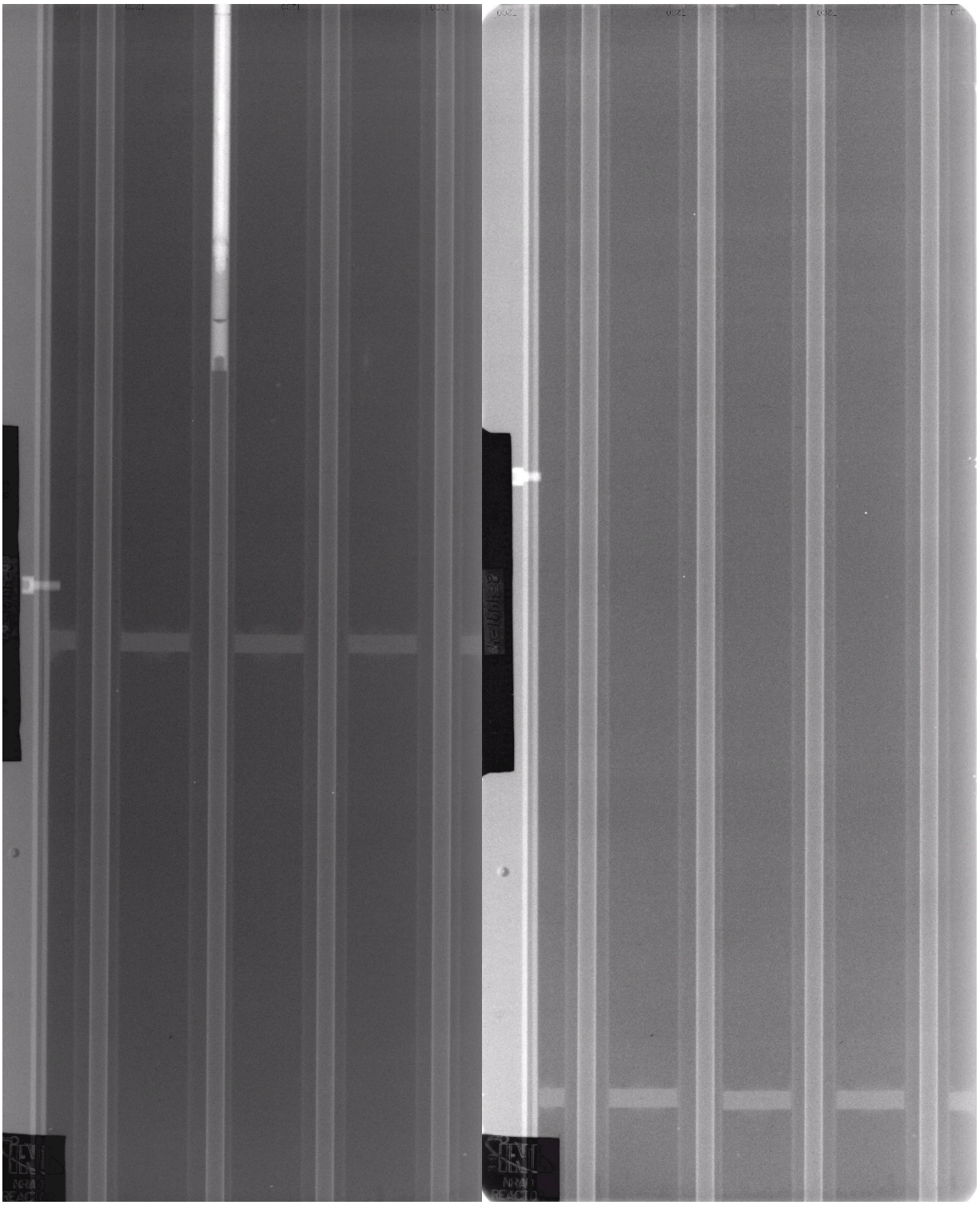

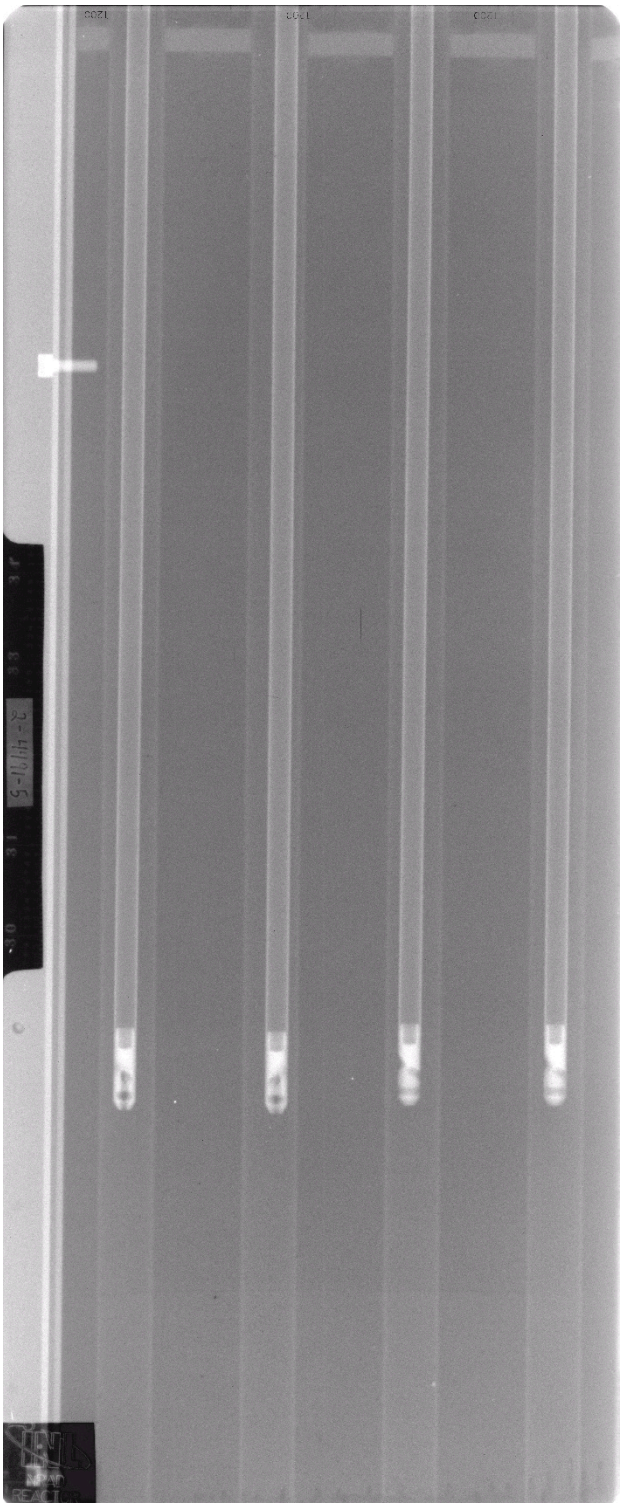

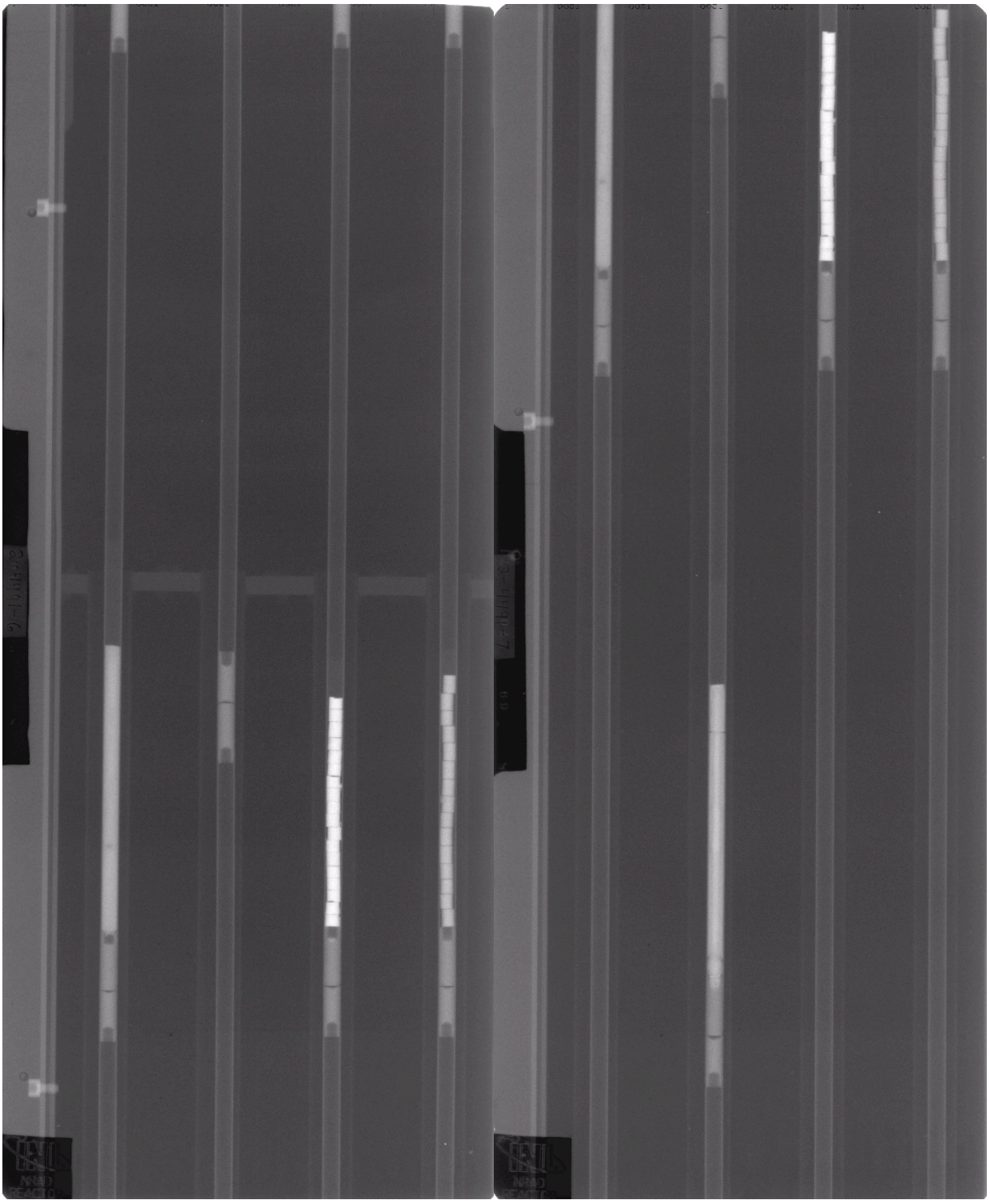

Epithermal Angle 2

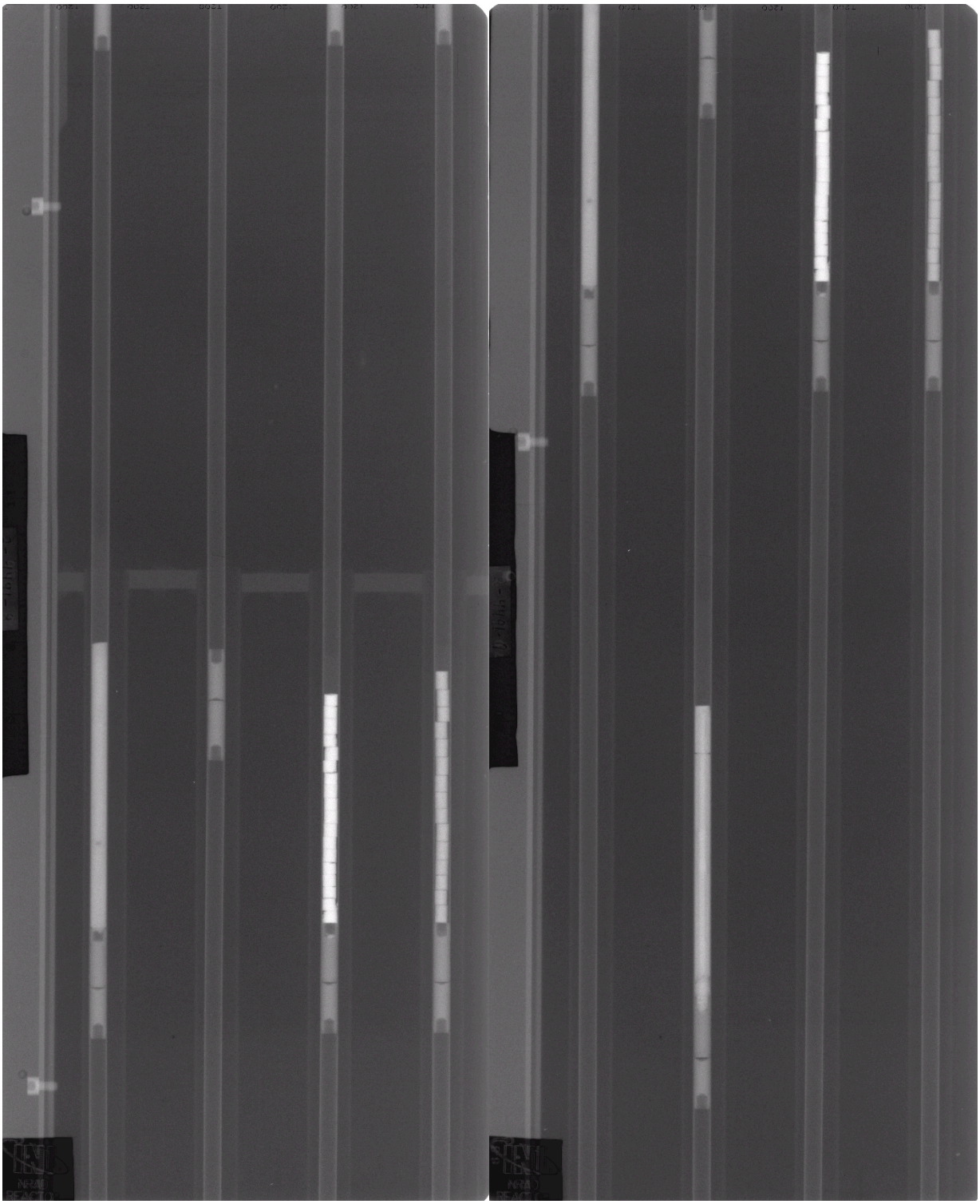

Appendix C

Complete Analytical Chemistry Results

Click on document to open pdf

INL - Materials and Fuels Complex

Analytical Laboratory

Final Report

AL Log #: 99526 **SPM #** **NA** 08-Aug-16 11:36

Login Name: BURNUP AND GAMMA SPECTROMETRY SAMPLES FOR FU **COC #:** NA

Requester: J. HARP, H. CHICHESTER **Charge #:** 102395191

Facility: HFEF, Bldg. 785 **Date Received:** 22-Feb-16 3:04:43 P

Approved by _____ **Date:** _____

Total Samples in Report: 1

Sample ID: KGT-2161

Where Taken: HFEF **Sampling Date:** 2/17/2016

Description: FUTURIX-FTA DOE1
CROSS SECTION PRE-IRRADIATION COMPOSITION:
U-28.3PU-3.8AM-2.1NP-31.7ZR
NUMBERS PRECEDING ELEMENTS DENOTE WEIGHT PERCENT, SUBSCRIPT NUMBERS REPRESENT MOLE PERCENT.

CLADDING IS Al

Analytical Method	Analyte	Result	Units	Error @ 2 Sigma
Gamma Spec				
	Ag-110m	<1e+1	uCi/Sample	N/A
	Am-241	1.17e+5	uCi/Sample	±6%
	Am-243	<5e+1	uCi/Sample	N/A
	Cd-109	<4e+2	uCi/Sample	N/A
	Ce/Pr-144	5.95e+3	uCi/Sample	±3%
	Co-60	3.38e+2	uCi/Sample	±3%
	Cs-134	9.48e+2	uCi/Sample	±3%
	Cs-137	5.73e+4	uCi/Sample	±4%
	Date & Time Cou	3-9-16 1232pm	NA	NA
	Eu-152	<4e+1	uCi/Sample	N/A
	Eu-154	1.95e+3	uCi/Sample	±3%
	Eu-155	1.16e+4	uCi/Sample	±3%
	Iso ID	Cm-243 5.51e+	uCi/Sample	±3%
	Mn-54	3.15e+2	uCi/Sample	±4%
	Nb-94	<8e+0	uCi/Sample	N/A
	Nb-95	<2e+1	uCi/Sample	N/A
	Pu-239	<1e+5	uCi/Sample	N/A
	Ru/Rh-106	1.76e+4	uCi/Sample	±3%
	Ru-103	<2e+1	uCi/Sample	N/A

INL - Materials and Fuels Complex

Analytical Laboratory

Final Report

AL Log #: 99527 **SPM #** **NA** 08-Aug-16 11:36

Login Name: BURNUP AND GAMMA SPECTROMETRY SAMPLES FOR FU **COC #:** NA

Requester: J. HARP, H. CHICHESTER **Charge #:** 102395191

Facility: HFEF, Bldg. 785 **Date Received:** 22-Feb-16 3:06:01 P

Approved by _____ **Date:** _____

Total Samples in Report: 1

Sample ID: KGT-2172

Where Taken: SOLID **Sampling Date:** 2/17/2016

Description: FUTURIX-FTA DOE2

CROSS SECTION PRE-IRRADIATION COMPOSITION:
PU-10.5AM-0.3NP-41.6ZR

NUMBERS PRECEDING ELEMENTS DENOTE WEIGHT PERCENT, SUBSCRIPT NUMBERS REPRESENT MOLE PERCENT.

CLADDING IS AIM

Analytical Method	Analyte	Result	Units	Error @ 2 Sigma
Gamma Spec				
	Ag-110m	<1e+1	uCi/Sample	N/A
	Am-241	3.13e+5	uCi/Sample	±5%
	Am-243	<2e+2	uCi/Sample	N/A
	Cd-109	<4e+2	uCi/Sample	N/A
	Ce/Pr-144	6.18e+3	uCi/Sample	±3%
	Co-60	2.94e+2	uCi/Sample	±3%
	Cs-134	1.00e+3	uCi/Sample	±3%
	Cs-137	7.27e+4	uCi/Sample	±4%
	Date & Time Cou	3-15-16 4:32p	NA	NA
	Eu-152	<5e+1	uCi/Sample	N/A
	Eu-154	9.06e+2	uCi/Sample	±3%
	Eu-155	8.87e+3	uCi/Sample	±4%
	Iso ID	Cm-243 9.95e+	uCi/Sample	±3%
	Mn-54	2.60e+2	uCi/Sample	±4%
	Nb-94	<6e+0	uCi/Sample	N/A
	Nb-95	<2e+1	uCi/Sample	N/A
	Pu-239	<2e+5	uCi/Sample	N/A

INL - Materials and Fuels Complex

Analytical Laboratory

Final Report

AL Log #: 99528 **SPM #** **NA** 08-Aug-16 11:36

Login Name: BURNUP AND GAMMA SPECTROMETRY SAMPLES FOR FU **COC #:** NA

Requester: J. HARP, H. CHICHESTER **Charge #:** 102395191

Facility: HFEF, Bldg. 785 **Date Received:** 22-Feb-16 3:06:52 P

Approved by _____ **Date:** _____

Total Samples in Report: 1

Sample ID: KGT-2180

Where Taken: SOLID **Sampling Date:** 2/17/2016

Description: FUTURIX-FTA DOE3

CROSS SECTION PRE-IRRADIATION COMPOSITION:
(U-0.51PU-0.27AM-0.14NP-0.08)N

NUMBERS PRECEDING ELEMENTS DENOTE WEIGHT PERCENT, SUBSCRIPT NUMBERS REPRESENT MOLE PERCENT.

CLADDIN

Analytical Method	Analyte	Result	Units	Error @ 2 Sigma
Gamma Spec				
	Ag-110m	<6e+0	uCi/Sample	N/A
	Am-241	5.28e+5	uCi/Sample	±5%
	Am-243	<2e+1	uCi/Sample	N/A
	Cd-109	<3e+2	uCi/Sample	N/A
	Ce/Pr-144	1.69e+3	uCi/Sample	±4%
	Co-60	7.01e+1	uCi/Sample	±4%
	Cs-134	2.69e+2	uCi/Sample	±3%
	Cs-137	4.68e+4	uCi/Sample	±4%
	Date & Time Cou	3-16-16 9:22a	NA	NA
	Eu-152	<2e+1	uCi/Sample	N/A
	Eu-154	1.34e+2	uCi/Sample	±5%
	Eu-155	3.64e+3	uCi/Sample	±3%
	Iso ID	Cm-243 1.67e+	uCi/Sample	±4%
	Mn-54	7.73e+1	uCi/Sample	±5%
	Nb-94	<4e+0	uCi/Sample	N/A
	Nb-95	<4e+0	uCi/Sample	N/A
	Pu-239	<1e+5	uCi/Sample	N/A

INL - Materials and Fuels Complex

Analytical Laboratory

Final Report

AL Log #: 99529 **SPM #** **NA** 08-Aug-16 11:36

Login Name: BURNUP AND GAMMA SPECTROMETRY SAMPLES FOR FU **COC #:** NA

Requester: J. HARP, H. CHICHESTER **Charge #:** 102395191

Facility: HFEF, Bldg. 785 **Date Received:** 22-Feb-16 3:07:38 P

Approved by _____ **Date:** _____

Total Samples in Report: 2

Sample ID: KGT-2193 FUEL FRACTION

Where Taken: HFEF **Sampling Date:** 2/17/2016

Description: FUTURIX-FTA DOE4

CROSS SECTION PRE-IRRADIATION COMPOSITION:
(PU-0.85AM-0.15)N+46.5ZRN

NUMBERS PRECEDING ELEMENTS DENOTE WEIGHT PERCENT, SUBSCRIPT NUMBERS REPRESENT MOLE PERCENT.

CLADDING IS

Analytical Method	Analyte	Result	Units	Error @ 2 Sigma
Gamma Spec				
	Ag-110m	<5e+0	uCi/Sample	N/A
	Am-241	2.50e+5	uCi/Sample	±5%
	Am-243	<6e+1	uCi/Sample	N/A
	Cd-109	<2e+2	uCi/Sample	N/A
	Ce/Pr-144	1.38e+3	uCi/Sample	±4%
	Co-60	7.19e+0	uCi/Sample	±10%
	Cs-134	2.39e+2	uCi/Sample	±3%
	Cs-137	3.94e+4	uCi/Sample	±4%
	Date & Time Cou	3-17-16 1:34p	NA	NA
	Eu-152	<2e+1	uCi/Sample	N/A
	Eu-154	1.19e+2	uCi/Sample	±4%
	Eu-155	2.93e+3	uCi/Sample	±4%
	Iso ID	Cm-243 7.48e+	uCi/Sample	±5%
	Mn-54	<4e+0	uCi/Sample	N/A
	Nb-94	<4e+0	uCi/Sample	N/A
	Nb-95	<4e+0	uCi/Sample	N/A
	Pu-239	<1e+5	uCi/Sample	N/A